Green Synthesis ZnO/TiO2 for High Recyclability Rapid Sunlight Photodegradation Textile Dyes Applications

Erviani Rusman
Hasanuddin University
Heryanto Heryanto
Hasanuddin University
Ahmad Nurul Fahri
Hasanuddin University
Inayatul Mutmainna
Hasanuddin University
Dahlang Tahir (dtahir@fmipa.unhas.ac.id)
Universitas Hasanuddin https://orcid.org/0000-0002-8241-3604

Research Article

Keywords: green synthesis, composite ZnO/TiO2, photocatalytic degradation, high recyclability, textile dye

Posted Date: April 13th, 2021

DOI: https://doi.org/10.21203/rs.3.rs-414953/v1

Green Synthesis ZnO/TiO_2 for High Recyclability Rapid Sunlight Photodegradation Textile Dyes Applications

Erviani Rusman, Heryanto Heryanto, Ahmad Nurul Fahri, Inayatul Mutmainna, Dahlang Tahir*

Department of Physics, Hasanuddin University, Makassar 90245, Indonesia

Corresponding authors email:*dtahir@fmipa.unhas.ac.id

Telp./Fax: +62-411-587634

Abstract. Composite ZnO/TiO_2 have been successfully synthesized by green synthesis method with various calcination temperature 500°C, 600°C, 700°C, and 800°C (TiO_2 concentrations: 2.5 g and 5 g) for photocatalyst application. In this study, *Calopogonium mucunoides* leaf extract was used as reducing and stabilizing agent. The synthesized composites were characterized by using Fourier Transform Infra-Red (FTIR), X-Ray Diffraction (XRD), and UV-Visible spectroscopy. The XRD spectra shows the hexagonal phase with wurtzite structure of ZnO and anatase for TiO_2. The best degradation performance is 98.26% (only 10 min) for ZnO/TiO_2 (5 g) with calcination temperature is 800°C. This is due to the highest distance between two optical phonon mode Δ(LO-TO) and lowest attenuating and propagating constant. The composite ZnO/TiO_2 shows high potentials photodegradation of organic dyes with the high stable recyclability up to 5 cycles (>95%) only for every 15 minutes. High potentials for applicability with the concept environmentally friendly principles and stability for circular chemistry, and efficiency of use the energy and chemicals.

Keywords: green synthesis, composite ZnO/TiO_2, photocatalytic degradation, high recyclability, textile dye.

INTRODUCTION

Hazardous contaminants in wastewater are affected by the textile industries, cosmetics manufacturing, pharmaceutical, metals industries, paper making, and agricultural industries [1-3]. Azo dye is a hazardous pollutant that contains (-N=N-) bond and phenyl or naphthyl group [4-6]. They are producing aromatic amines during the decomposition process and potentially cause carcinogenic and mutagenic. On the other hand, the presence of azo dye in water causes severe effects on clean water availability and the environment [5-8]. The type of azo dyes is a mono-azo dye (methylene blue, methylene orange, AO7 (acid orange 7)), diazo dye (congo red, 6B (direct lake blue)), and poly azo dyes (direct black BN) [6]. One of the most widely used azo dye is Congo Red (CR). CR is used in processing textile, paper, cosmetic, and pharmaceutical industries [9,10]. Those dye are difficult to degrade to be a severe issue for environmental and human health. The increased contaminant compounds in wastewater are interested researchers in finding the polluted water treatment method to provide clean and healthy water [11].

Water purification methods were varied through a physical, biological, and chemical process [12,13]. The photocatalyst is one of the most effective and simple techniques used in water treatment because it removes organic contaminants easily [11, 14,15]. Green synthesis is used as an alternative method to produce nanoparticles for photocatalyst applications. It has several advantages, such as eco-friendly, and it does not produce second contaminants [3]. This method used extracts of various plants as reducing or stabilizing agents. Plant extract contains phytochemicals that act as bio-reduction materials for capping agents in particular nanoparticles' synthesis process [16]. The reported materials nanoparticles have been produced by using green synthesis are: Au, Ag, Pt, Pd, α-Fe_2O_3, CeO_2-, ZnO, TiO_2, ZrO_2, and SnO_2 [19-22]. TiO_2 and ZnO are

chemically stable semiconductors that can produce an active charge during irradiation by light with suitable wavelengths [12,23,24]. Zinc oxide is n-type semiconductor with high excitation binding energy, bandgap width (3,37eV for anatase phase), biocompatibility, and it is more active when irradiation by visible light. Irradiation process for ZnO will create electron-hole by gain energy of electron for exciting to the conduction band [1]. The electron at the conduction band moves easily to the valence band by the recombination processes. The heterostructure method is effective approach to control and minimize the recombination rate in ZnO consequently increase the charge carrier lifetime [25-28].

The TiO_2 is an effective semiconductor that combines with ZnO nanoparticles displays improvement in photocatalytic activities [29-35]. TiO_2 has higher efficiency as a photocatalytic because it is responsive to the visible spectrum with bandgap 3.2 eV [36-41]. It is using as a photocatalytic due to its good optical properties, low cost, and high chemical stability [40-42]. The catalyst was used for photodegradation of chemical or organic pollutants in wastewater under visible irradiation [43,44]. Doping TiO_2 with metals or non-metal ions will increase the visible light absorbance capacity or reactivity in the UV wavelength [45,46]. The previous reports for ZnO/TiO_2 as a photocatalysis with various synthesized methods are: ZnO/TiO_2 nanohybrids by using a hydrothermal method for MB, R6G, OTC degradation [1], ZnO/TiO_2 by using solid-state for quinoline degradation [29], ZnO/TiO_2 by using sol-gel for dye degradation of methylene blue [13,35], ZnO and TiO_2 commercial for phenothiazine decolorization [36], and ZnO/TiO_2 thin film by using the hydrothermal method for orange G degradation [10]. However, the green, appropriate, and efficient photocatalysts materials that can be easily integrated into wastewater plants and reused for real

applications is crucial. The principles process of synthesized these photocatalysts materials should be environmentally friendly, circular chemistry, and increasing the efficiency of the use of energy and chemicals.

For environmentally friendly materials, we synthesize ZnO/TiO_2 using *Calopogonium mucunoides* leaf extract by green method. *Calopogonium mucunoides* is a legume and easily grow were impacting agricultural if growth uncontrolled and semi-natural ecosystems which becoming an environmental problem mainly in Indonesia. By using this type of a legume for photocatalyst, means that contributes to the green environment, low-cost fabrication, efficient, recyclable, and applicability in short time to produce clean water from decontaminant. In this study, a facile, suitable for mass-productive, green, and cost-effective method for the fabrication of nanohybrid ZnO/TiO_2 photocatalyst for enhanced visible-light was developed. The process of photocatalyst materials potentials to be holistically integrates with environmentally friendly principles, circular chemistry, and efficiency of use the energy and chemicals [47-49].

The ZnO/TiO_2 composites for concentration of TiO_2 are 2.5 g and 5 g, and various calcination temperatures (500^{o}C, 600^{o}C, 700^{o}C, and 800^{o}C) characterized by using XRD, FTIR, and UV-Vis spectroscopy. The XRD spectra used for analysis the structural properties and FTIR spectra for the optical properties in the form of the refractive index (n) and extinction coefficient (k) by applying Kramers Kronig (KK) relation. The longitudinal and transversal optical phonon mode, the complex dielectric function (real part (ε_1) and imaginary part (ε_2)), energy loss function (Im (-1/ ε)), and the optical absorption coefficient were determined from the n and k. The photocatalyst efficiency for degradation of CR were analysis using UV–Vis spectrometer spectra.

High recyclability of the ZnO/TiO_2 composites as catalyst in photodegradation processes are also reported in this study.

EXPERIMENTAL

Materials and Preparation Sample

Calopogonium mucunoides (CM) leaves were taken from the Enrekang district, South Sulawesi, Indonesia. Zinc acetate dihydrate ($Zn(CH_3COO)_2 \cdot 2H_2O$) (Merck), titanium dioxide (TiO_2) (Merck), and natrium hydroxide (NaOH) (Merck), and congo red ($C_{32}H_{22}N_6Na_2O_6S_2$) (Merck).

The CM leaves were washed several times by distilled water to remove debris and dirt, then dry them at room temperature for one week. The leaves were powdered using blender and sieved the powder with 100 Mesh for uniform size. The extract was prepared by adding 5 g of CM leaves powder in 100 ml distilled water and stirred at 80^{o}C for 20 minutes. It was filtered with Whatman No.1 filter paper. The filtrate was used for synthesis ZnO/TiO_2, for more detail illustration of synthesized processes see **Figure 1**.

Synthesis of ZnO/TiO_2

Sol gel method was used for green synthesis ZnO/TiO_2. The solution prepared with 20 ml CM leaf extracts, 80 ml distilled water, and 5 g $Zn(CH_3COO)_2 \cdot 2H_2O$ as a precursor. It was stirred at constant temperature 95^{o}C and speed 500 rpm. After 15 minutes heated, TiO_2 was added to the zinc oxide solution. TiO_2 solution was prepared 2.5 g and 5 g TiO_2 powder by added 10 ml distilled water, then homogenized for 5 minutes by constant stirring at 200 rpm using magnetic stirrer. NaOH was added

dropwise to the solution till pH 7. The paste was formed after continuous heating and stirring for overnight. The sample paste was evaporated at 80ºC for 10 hours and continue calcined for 2 hours at the temperature 500ºC, 600ºC, 700ºC, and 800ºC to obtain ZnO /TiO_2 powder, the illustration procedure as shown in **Figure 2**.

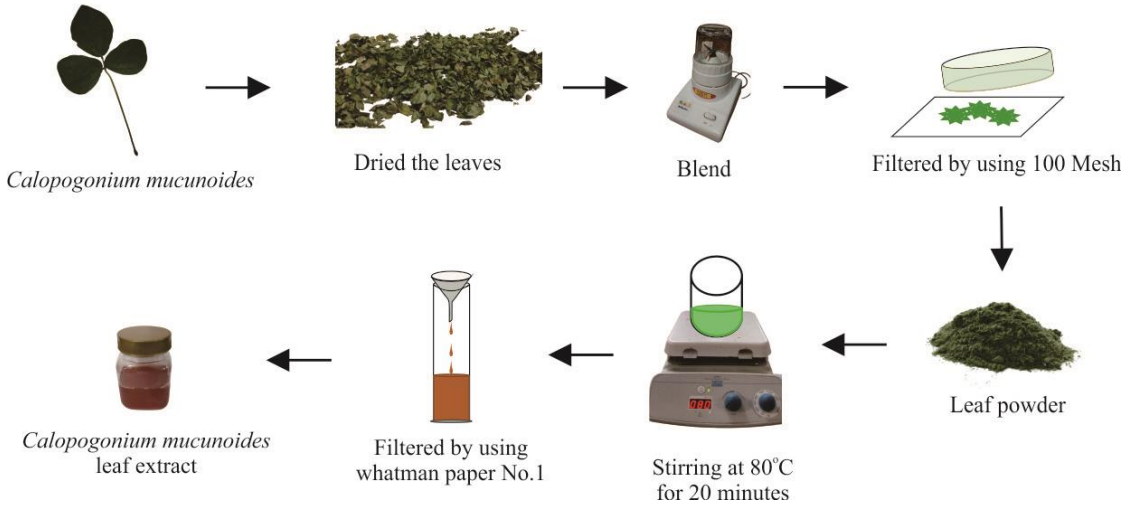

Figure 1. Schematic illustration for extraction of *Calopogonium mucunoides* leaves

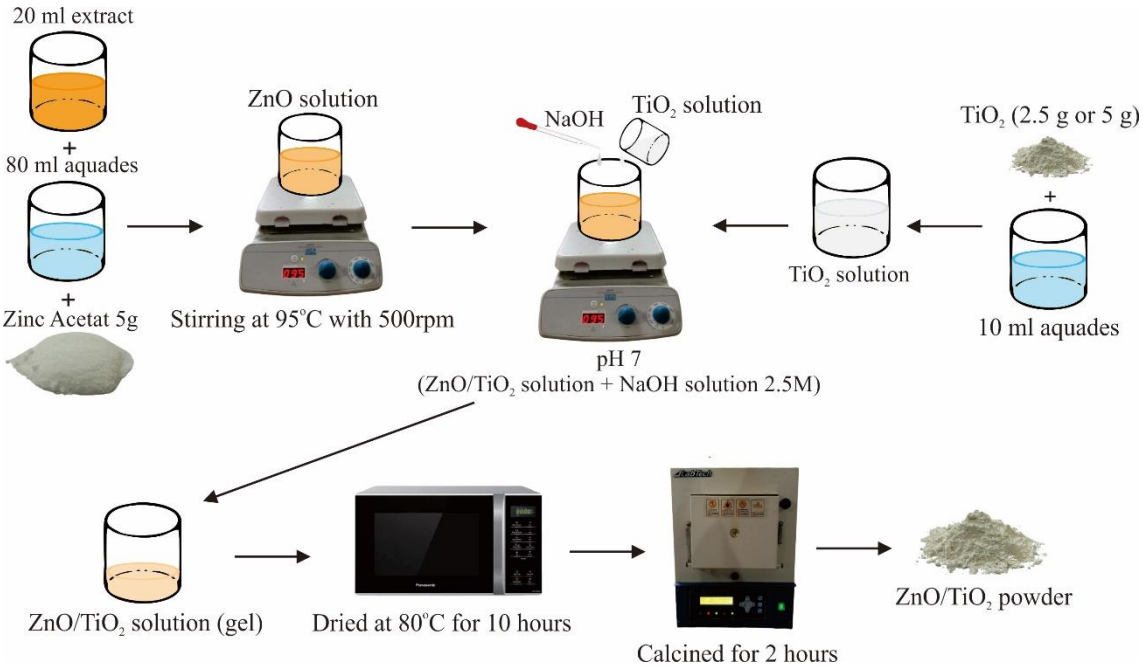

Figure 2. Illustration procedure of green synthesis ZnO/TiO_2 using *Calopogonium mucunoides* leaf extract

Characterization

The synthesized powder was characterized by XRD spectroscopy, FTIR spectroscopy, and UV-Vis spectrophotometer. XRD spectroscopy (Shimadzu 700) with CuKα radiation at wavelength (λ) 1.54 Å ($25^o \leq 2\theta \leq 65^o$, *40kV, 30 mA, scan rate 2* min^{-1}, *step size* 0.02^o) was used to determine the structure and crystallite size of the samples by using Debye Scherrer formula. Fourier Transform Infra-Red Spectroscopy (FTIR Spectroscopy) (*IRPrestige-21 (Shimadzu Corp.)*) to analyze the functional groups that present and optical properties of the samples. UV-Vis spectrophotometer (*Shimadzu UV-Vis Spectrophotometer UV-1800*) was used to study the photocatalytic activity of CR.

Photocatalytic Mechanism

The photocatalytic degradation procedure consisted of adding 0.02 g of ZnO/TiO_2 powder into 100 ml of CR solution (40 mg/L). The solution was stirred and exposed to light using 300W Osram Tungsten Halogen lamp as a light source. To analyze the CR concentration after degradation process, the solution was carried out every 5 minutes and filtered it. Concentration of the solution after the degradation process was determined by using UV-Vis spectrophotometer and the percentage of degradation determined by:

$$D\ (\%) = \left(\frac{C_0 - C_t}{C_0}\right) \times 100\% \quad (1)$$

where D (%) is the percentage of degradation, C_0 is the initial concentration (at t is 0 min), and C_t is the concentration after time irradiation *t* min.

The recyclability of composite in photodegradation was studied by using ZnO/TiO_2 (2.5 g) at temperature 500ºC. The 0.04 g of ZnO/TiO_2 was added into 100 ml CR solution (40 mg/L). The solution was stirred at 150 rpm by using *magnetic stirrer* and it was irradiated for 15 minutes. The solution was filtered, and the concentration was analyzed by using UV-Vis spectrophotometer. The composite was washed with distilled water and centrifuged at 1500 rpm within 5 minutes. These steps were applied repeatedly for 5 times. The sediment was dried at 80ºC within 10 minutes. Dried composite was added back into 100 ml CR solution. It was repeated for five cycles.

RESULTS AND DISCUSSION

XRD analysis

The XRD spectra were used to identify the crystalline phase of composites ZnO/TiO_2 extracted by green synthesis mediated by *Calopogonium mucunoides* leaf. **Figure 3** shows XRD diffraction patterns for composite ZnO/TiO_2 (TiO_2 is 2.5 g and 5.0 g) at various calcination temperature. For all samples shows several diffraction peaks 2θ of ZnO at 31.84º, 34.48º, 36.36º, 47.68º, 56.74º, and 62.98º which correspond to the crystal planes (100), (002), (101), (102), (110), and (103) based on JCPDS card no: 36-1451 [50]. The presence of TiO_2 in the composite ZnO/TiO_2 was confirmed by the peaks 2θ at 25.38º, 37.94º, 47.64º, and 62.96º which correspond to the crystal planes (101), (004), (200), and (204) for structure anatase based on JCPDS card no: 21-1272 [51] as can be seen in **Figure 3 (a)** and for TiO_2 is 5 g in **Figure 3 (b)**.

Figure 3 (c) and **(d)** shows enlarger XRD spectra for diffraction peak from 30° to 37 ° for various calcination temperature. It shows there are shifts toward the highest of the diffraction angle for 2.5 gr TiO_2 at 600°C and 700°C due to the lattice reduction and for 800°C small shits backward to the lower of the diffraction angle due to the some of the atoms are uniform arrangement and forming new cluster crystal [52-54]. For composite with 5.0 g TiO_2 shows shifts to the higher diffraction angle regularly due to the number of atoms Ti filled the lattice of ZnO over than the capacity for the lattice reduction or may due to the large ionic radius of Ti compared with that of Zn [55].

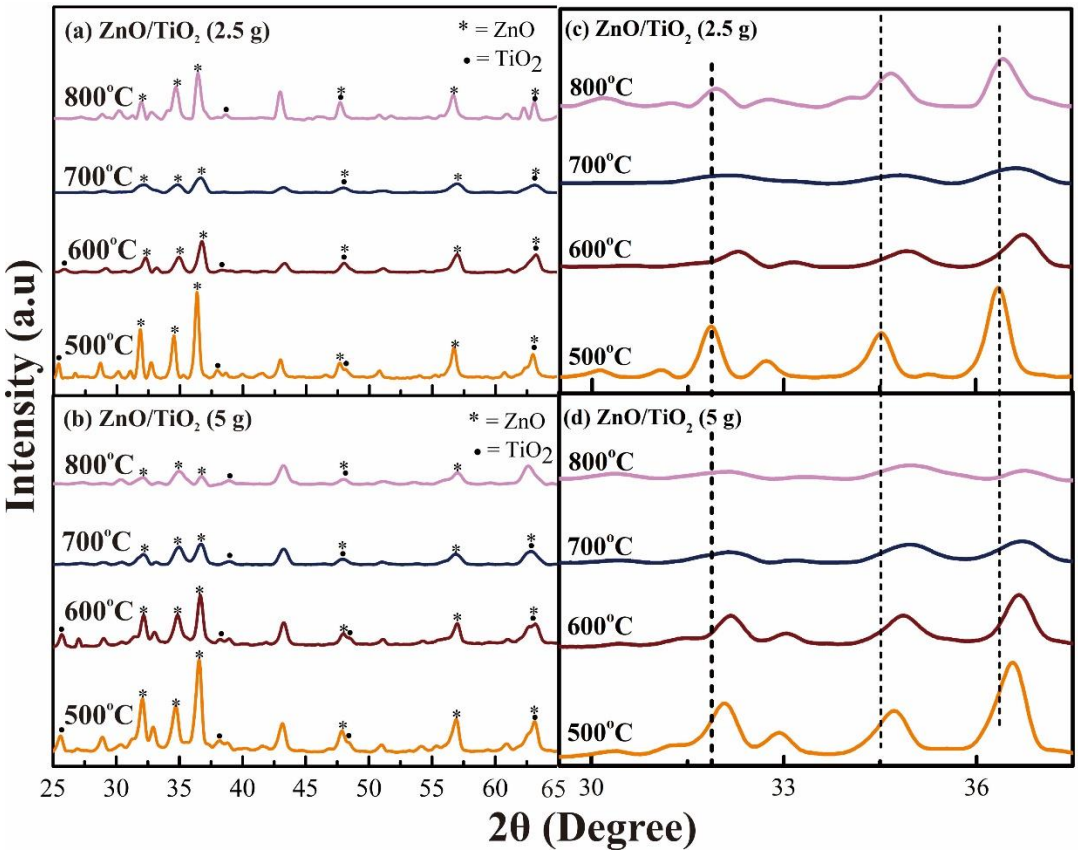

Figure 3. XRD analysis of ZnO/TiO_2 synthesized from *Calopogonium mucunoides* leaves extract for various calcination temperature (500°C, 600°C, 700°C, 800°C) and TiO_2 concentration (2.5 g and 5 g)

The intensity (101) crystal plane of TiO_2 clearly can be seen in composite at the temperature ≤ 600ºC but for > 600ºC the intensity peak reduces drastically or almost disappears may due to the phase change from TiO_2 to $ZnTiO_3$. In addition, the (102) and (103) planes of ZnO overlap with the (200) and (204) planes of TiO_2. It shows that there is perfect interaction occurs between the lattice of ZnO and TiO_2 to produce ZnO/TiO_2 composite [56]. At the lowest temperature, there are some small peaks that occur at 2θ: 30.14º, 42.96º, 50.78º, and 60.70º correspond to the crystal plane (220), (400), (422), and (440), respectively, identified $ZnTiO_3$ phase based on the JCPDS card No: 39-0190 [57]. For the temperature increases from 500ºC to 600ºC, the diffraction peaks intensity of $ZnTiO_3$ were decrease and the phase transformation occurred at the temperature 800ºC clearly can be seen the intensity of $ZnTiO_3$ decreases and Zn_2TiO_4 increase. It shows that some of the $ZnTiO_3$ phase were decomposed to forming Zn_2TiO_4 phase as can be seen at the diffraction peaks 32.24 º, 34.90 º, 36.82 º, and 56.96º based on the JCPDS: 01-073-0578 [11,14,58]. The peak intensities decrease and the width of FWHM increase by increasing the calcination temperature from 600ºC to 700ºC may due to the crystallite size or the interatomic spacing decreased [14,59].

Table 1. The average crystallite size, dislocation density, and strain determined by the quantitative analysis of XRD spectra in Figure 3.

Sample	Temperature (°C)	Average crystallite size (nm)	Dislocation density (nm^{-2})	Strain (S)
ZnO/TiO_2 (2.5 g)	500	19.99	0.0025	0.0048
	600	11.87	0.0071	0.0081
	700	7.62	0.0172	0.0132
	800	17.64	0.0032	0.0057
ZnO/TiO_2 (5 g)	500	15.73	0.0040	0.0062
	600	15.21	0.0043	0.0063
	700	8.86	0.0127	0.0111
	800	8.94	0.0125	0.0120

From the XRD spectra in **Figure 3** clearly shows relationship between calcination temperatures with the peak intensities. At low calcination temperature (500°C) the intensity of diffraction peaks are sharp and decrease with increasing the calcination temperature, consequently decrease the crystallite size as can be seen in **Table 1** calculated from the Debye Scherrer's equation [3,60,61]:

$$\Gamma=\frac{K.\lambda}{\beta.Cos\ \theta} \quad (2)$$

where Γ is the crystallite size, θ is the Bragg diffraction angle, K is the constant about 0.9, λ is the wavelength of X-ray (for Cu is 1.5406 Å), and β is full width at half-length maximum (FWHM). The average of crystallite size, dislocation density, and strain were shown in the **Table 1**.

FTIR analysis

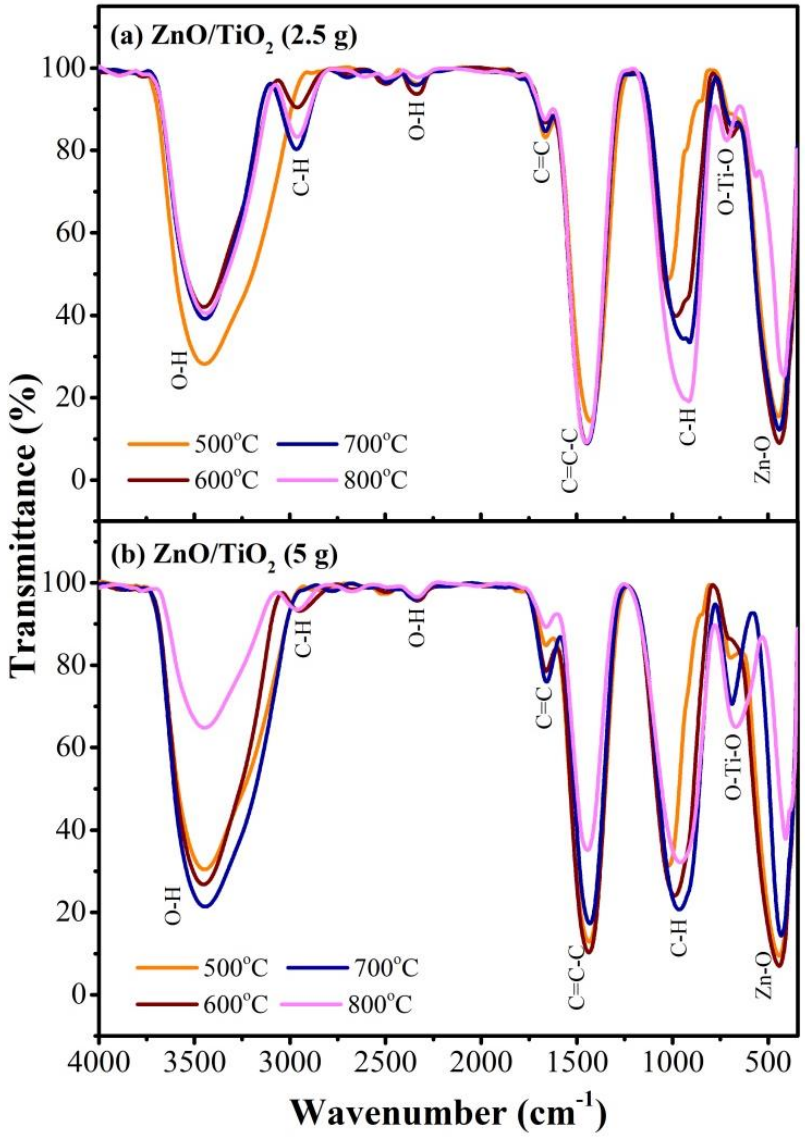

Figure 4. FTIR spectra of ZnO/TiO_2 synthesized from *Calopogonium mucunoides* leaves extract for various calcination temperature (500ºC, 600ºC, 700ºC, 800ºC) and TiO_2 concentration (2.5 g and 5 g)

Figure 4 shows FTIR spectra at the wavenumber 350-4000 cm^{-1} for identified the functional groups and vibrational bonds of composite ZnO/TiO_2. The peak 446 cm^{-1} corresponding to the vibration bond of Zn-O [3,62]. The peak at 723 cm^{-1} correspond to the O-Ti-O band [63]. The function group of C-H band at the wave number 1000-1100

cm^{-1} [14] and at the wavenumber 1447 cm^{-1} and 1665 cm^{-1}, there are chemical bonds of C=C-C and C=C tensile vibration, respectively [21,55]. O-H bond appears at the wavenumber 2504 cm^{-1} and 3455 cm^{-1} corresponding to vibration band from suspension of hydroxyl group in adsorbed water [3,64]. A weak infrared peak at 2338 cm^{-1} probably due to the CO_2 vibration bond absorbed during calcination process. The peak at 2968 cm^{-1} is mainly due to the stretching vibration of C-H bond from the absorption of the alkane groups [14].

Optical properties

The optical properties (refractive index (n) and extinction coefficient (k)) were determined from the quantitative analysis of FTIR spectra by applying K-K relation [65-67]. For the analysis optical properties, we have used only wavenumber in the range from 860 cm^{-1} to 1115 cm^{-1} due to the C=C-C bonding which probably come from the green synthesis methods. The FTIR spectra form the equipment is in the form of transmittance (T(ω)), where need to be converted to the reflectance (R(ω)) [68] by the relations:

$$A(\omega)=2-\log[T(\omega)\%] \tag{3}$$

$$R(\omega)=100-[T(\omega)+A(\omega)] \tag{4}$$

The reflectance R(ω) as a function of the wavenumber is substitute in the following equations for determining the optical properties (refractive index for real part n(ω) and extinction coefficient for imaginary part k(ω)) [68]:

$$n(\omega)=\frac{1-R(\omega)}{1+R(\omega)-2\sqrt{R(\omega)}\cos\emptyset(\omega)} \tag{5}$$

$$k(\omega)=\frac{2\sqrt{R(\omega)}\cos\emptyset(\omega)}{1+R(\omega)-2\sqrt{R(\omega)}\cos\emptyset(\omega)} \tag{6}$$

φ(ω) is the phase change from the incident photon beam bombardment to the sample and traveling at the surface down to few atoms at the sample and then reflected photon beam out which calculated by the following equation:

$$\varphi(\omega)=-\frac{\omega}{\pi}\int_0^{\infty}\frac{\ln R(\omega')-\ln R(\omega)}{\omega'^2-\omega^2} \quad (7)$$

For easily computational of by φ(ω), the K-K (Kramers-Kronig) relation was used and the new equation of phase change φ(ω):

$$\varphi(\omega)=-\frac{4\omega_j}{\pi}\Delta\omega\ \sum_i\frac{\ln(\sqrt{R(\omega)})}{\omega_i^2-\omega_j^2} \quad (8)$$

where $\Delta\omega=\omega_{i+1}-\omega_i$ and j is series of wavenumber, if j is an odd number, so then i parts is 2,4,6,8,…,j-1, j+1 and while wavenumber j is an even, i parts is 1,3,5,7,…,j-1, j+1.

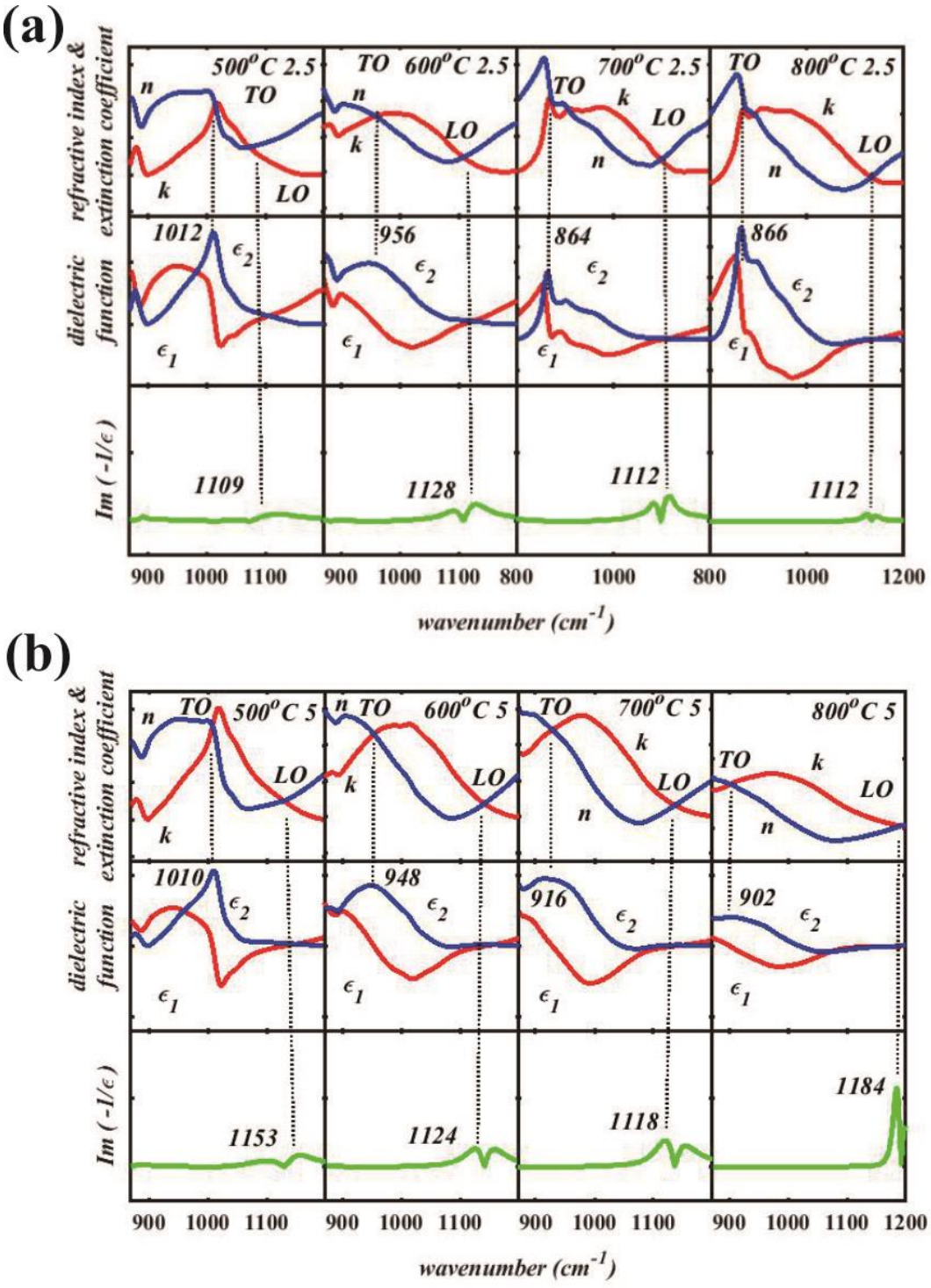

Figure 5. The optical properties (refractive index (n) and extinction coefficient (k)) determined from the FTIR spectra in Figure 4, from the optical properties the dielectric function, the energy loss function Im $(-1/\varepsilon_1(\omega))$ are determined for various calcination temperature for (a) ZnO/TiO_2 (2.5 g) and (b) ZnO/TiO_2 (5 g).

Figure 5 (a and b) shows the intersection at higher wavenumber indicated by LO and intersection point at the lower wavenumber indicated by TO and the values are presented in **Table 2**. **Figure 5(a)** depicts the transverse optical (TO) of ZnO/TiO_2 (2.5 g) shifts to the lower wavenumber by increase the calcination temperature up to 700 ^oC, but for 800^oC the TO shifts to the higher wavenumber may due to the effect of the weak strain in the crystal structure. **Figure 5(b)** shows TO was decreased with increasing the temperature. In this study, the highest distance between the two optical phonon vibration mode (Δ(LO-TO)) for ZnO/TiO_2 (5 g) at 800^oC may due to some H_2O loses in the lattice consequently increase optical bandgap [64,69]. The Δ(LO-TO) was increased with the increasing the TiO_2 concentration at the same calcination temperature but not for 700^oC may due to the number of defect (dislocation density) increase consequently the atomic bonding unstable and rearrange to form new atomic cluster in the lattice structure [70,71].

Table 2. Transverse optical (TO) phonon mode, longitudinal optical (LO) phonon mode, and Δ(LO-TO)

Sample	Temperature (°C)	TO (cm^{-1})	LO (cm^{-1})	Δ(LO-TO) (cm^{-1})
ZnO/TiO_2 (2.5 g)	500	1012	1109	97
	600	956	1128	172
	700	864	1112	248
	800	866	1112	246
ZnO/TiO_2 (5 g)	500	1010	1153	143
	600	948	1124	176
	700	916	1118	202
	800	902	1184	282

The real part (ε_1) and imaginary part (ε_2) of dielectric function functions were calculated from the relation between *n* and *k* as follows [66]:

$$\varepsilon_1(\omega)=n^2(\omega)-k^2(\omega) \quad (9)$$

$$\varepsilon_2(\omega)=2n(\omega)k(\omega) \quad (10)$$

The main peak position of the imaginary part (ε_2) and the energy loss function Im ($-1/\varepsilon_1(\omega)$) were used for confirmation of the TO and LO phonon vibration modes from the intersection point between *n* and *k*, respectively. These finding shows consistency result as can be seen in the **Figure 5**, indicated that the effectiveness of the FTIR spectra for determining optical properties and for identification optical phonon modes. The energy loss function also identified as a plasma frequency as reported in Ref. [65,66,72] from the quantitative analysis of electron spectroscopy [66,73]. The Δ(LO-TO) is important parameters to identified stability of the covalent bond and the lattice match in the ZnO/TiO_2 composite [70].

The next important parameters are attenuation constant α and propagation constant β which determined from the following relations:

$$\alpha = \omega \sqrt{\frac{\mu_0 \varepsilon_0 \varepsilon_{1(\omega)}}{2} \left[\sqrt{1 + \left(\frac{\varepsilon_2(\omega)}{\varepsilon_1(\omega)} \right)^2} - 1 \right]} \tag{11}$$

$$\beta = \omega \sqrt{\frac{\mu_0 \varepsilon_0 \varepsilon_{1(\omega)}}{2} \left[\sqrt{1 + \left(\frac{\varepsilon_2(\omega)}{\varepsilon_1(\omega)} \right)^2} + 1 \right]} \tag{12}$$

where μ_0 is a constant related to the permeability and ε_0 is also constant for permittivity in a free space.

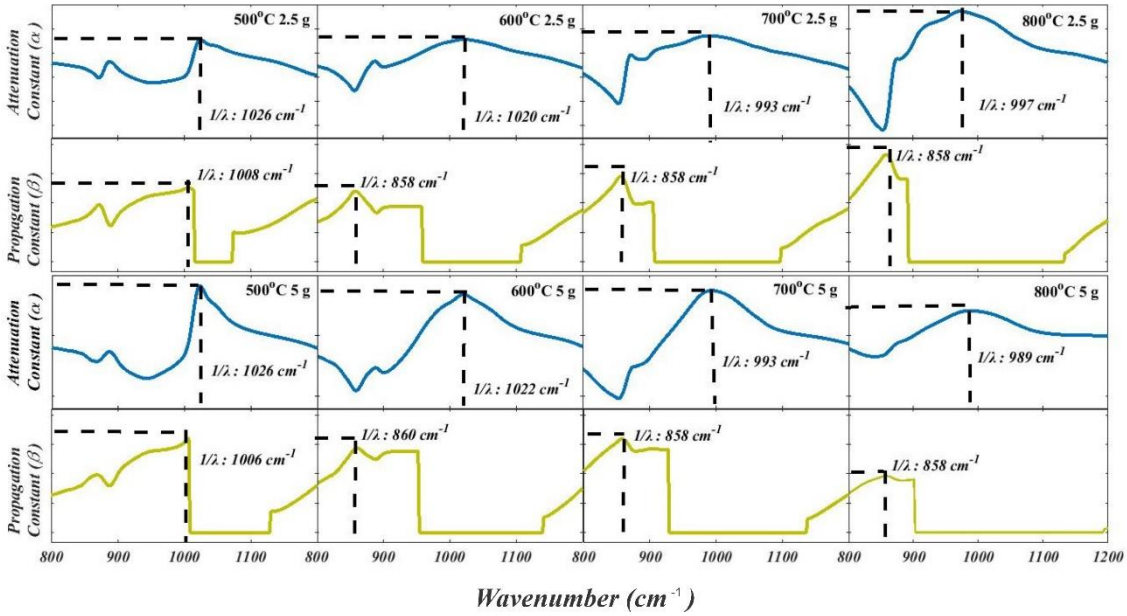

Figure 6. Attenuation constant (α) (first and third rows) and propagation constant (β) (second and fourth rows) as a function of the wavenumber for calcination temperature from 500°C (left) to 800°C (right). First and second rows for 2.5 gr of TiO_2 in ZnO/TiO_2 composite and the third and fourth rows for 5 gr of TiO_2 in ZnO/TiO_2 composite.

For 2.5 gr of TiO_2 in ZnO/TiO_2 composite shows the attenuation and propagation constant increase with increasing the calcination temperature from 500°C (left) to 800°C (right) and opposite trend for 5 gr of TiO_2 in ZnO/TiO_2 composite as can be seen in **Figure 6**. The best composite for photocatalyst is for low attenuating and propagating constant, means that the structure will easily suppressing recombination of the charge particle due to the higher strain between the atoms [52, 54]. In this study shows 5 gr of TiO_2 in ZnO/TiO_2 composite high potentials compared than that of 2.5 gr TiO_2 in ZnO/TiO_2 composite for the same calcination temperature [64].

Bandgap and Photocatalytic Degradation

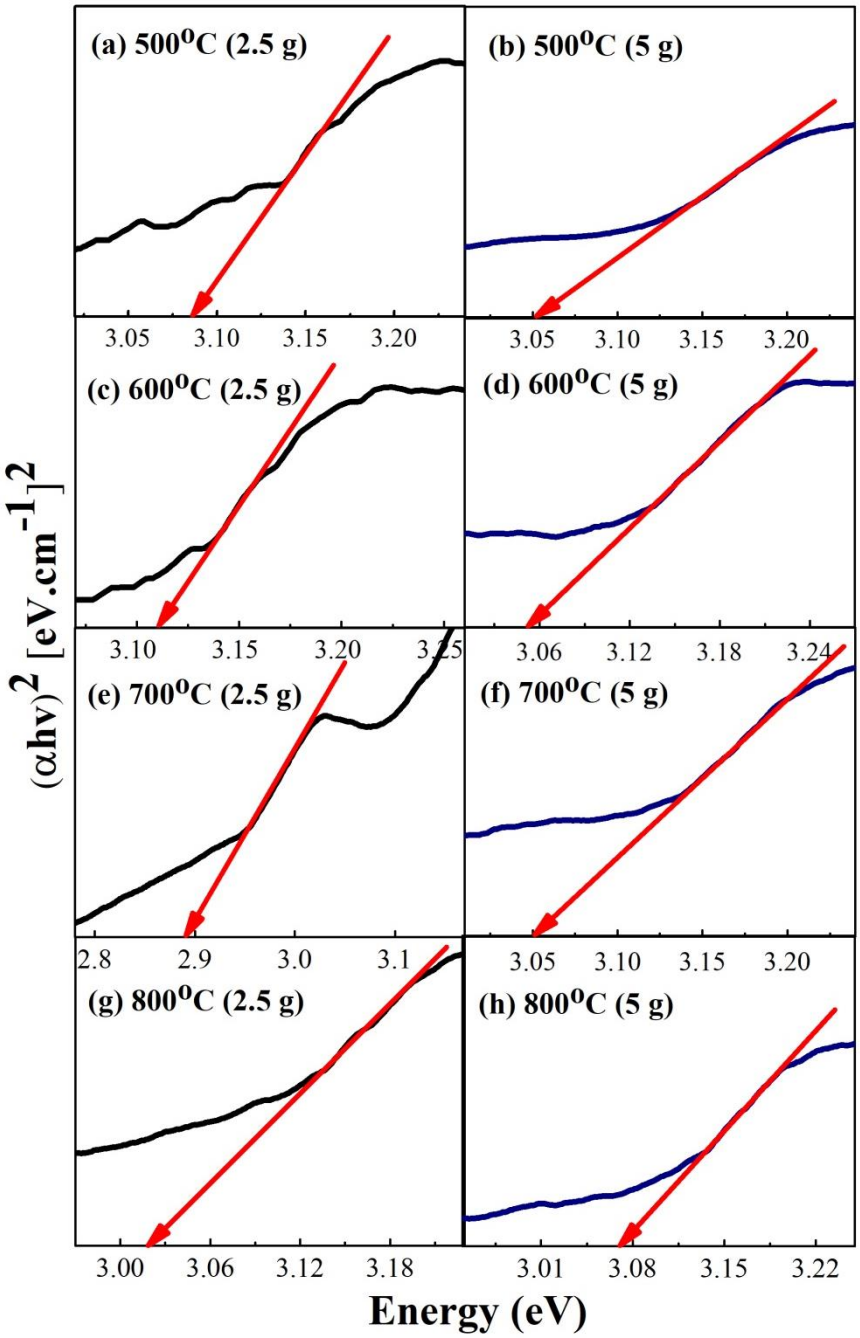

Figure 7. Band gap of ZnO/TiO_2 synthesized from *Calopogonium mucunoides* leaves extract for various calcination temperature (500°C, 600°C, 700°C, 800°C) and TiO_2 concentration (2.5 g and 5 g)

Band gap of ZnO/TiO_2 composites indicated by the arrows at the absorbance spectra in **Figure 7**. Band gap values were obtained by using Touch Plot method and the corresponding results are presented in **Table 4**, which determined by the relation as follows:

$$(\alpha h\nu)^{1/m} = C(h\nu - E_g) \quad (13)$$

where α is absorption coefficient, $h\nu$ refers to photon energy, C is band form parameter, m=1/2 for the direct allowed transition, and E_g is band gap energy.

The calcination temperature from 500°C to 700°C, the band gap of composite ZnO/TiO_2 for 5 g TiO_2 is same but for composite with 2.5 g TiO_2 is fluctuates due to the effect of cohesion force between the atoms of Zn and Ti. For calcination temperature from 700°C to 800°C, the sample for the different concentration of TiO_2 shows increases the band gap may due to the effect of particle size and crystal phase in the composite is increase [14,74].

The ability of ZnO/TiO_2 as photocatalytic materials for degradation of CR was analyzed using UV-Vis spectrophotometer. **Figure 8** shows the absorbance spectrum of CR with ZnO/TiO_2 during irradiation, for the solution can be identified visually or by the absorbance spectra at the wavelength 400-600 nm. The time for every sample to degrade CR was different, it influenced by the ability of charge particle to produce hydroxyl and superoxide radical which play the important roles in photodegradation.

The relation between the percentages of degradation with irradiation times are shown in **Figure 9** and the corresponding results of percentage degradation for all sample with various calcination temperature and various TiO_2 concentration were shown in **Table 3**. The efficiency of photocatalyst ZnO/TiO_2 mediated by *Calopogonium mucunoides* leaves extract is higher than 94%. The highest efficiency is

98,26% that obtained by ZnO/TiO_2 (5 g) with calcination temperature is 800°C. It indicates the synthesis composites ZnO/TiO_2 have a great potential for photocatalytic materials.

Photocatalytic activity was affected by some factors: type of photocatalyst material, crystallite size, and agglomeration level. It means that, the photodegradation process may related to the different competing factors [14]. Based on the previous reported which published by Selvi et.al, a diminution of the crystallite size led to an increase in the specific surface area that could enhance the active reaction of the photocatalyst materials [75].

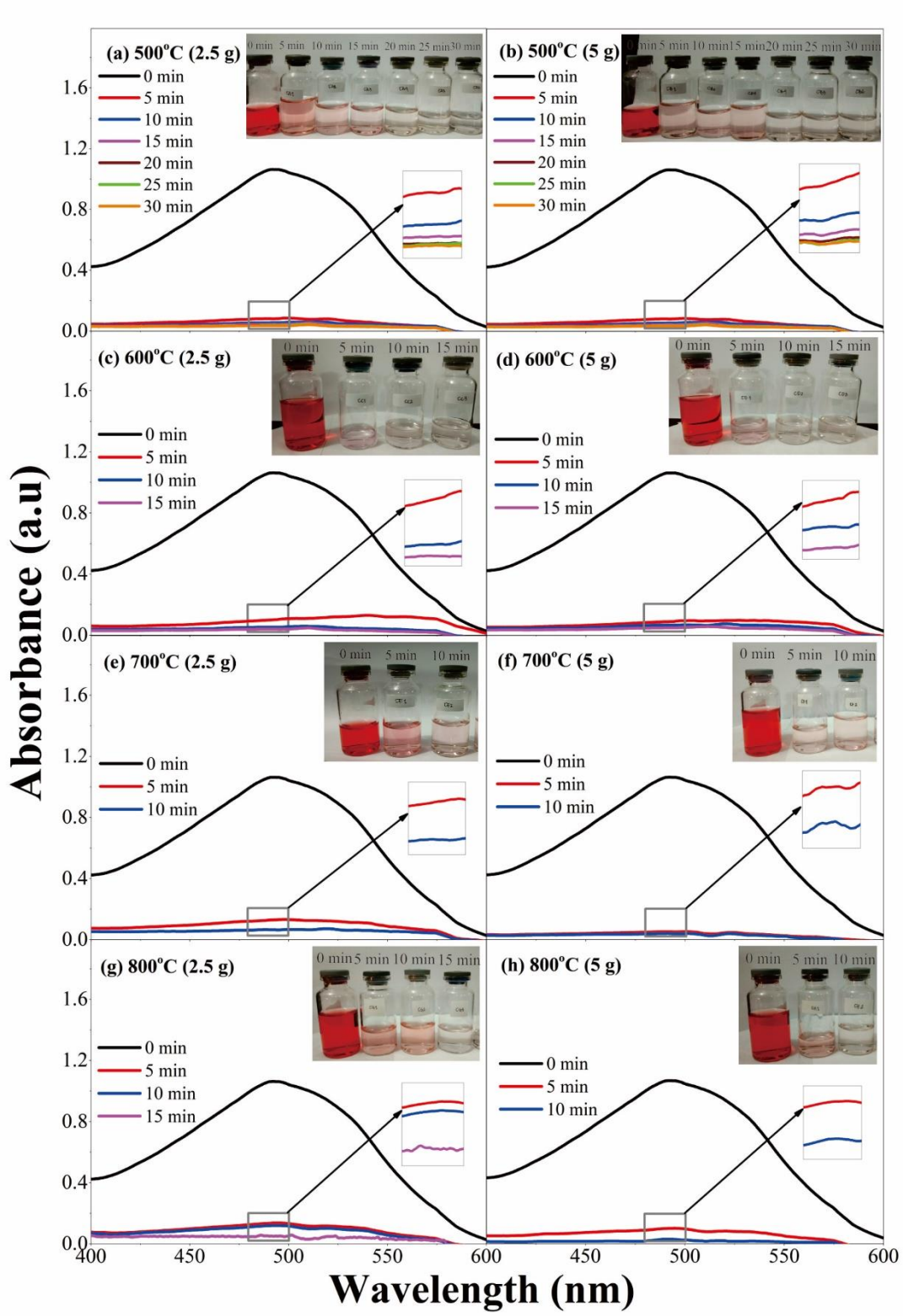

Figure 8. UV-visible absorption spectra of ZnO/TiO_2 (2.5 g and 5 g) synthesized from *Calopogonium mucunoides* leaves extract for various calcination temperature (500°C, 600°C, 700°C, and 800°C)

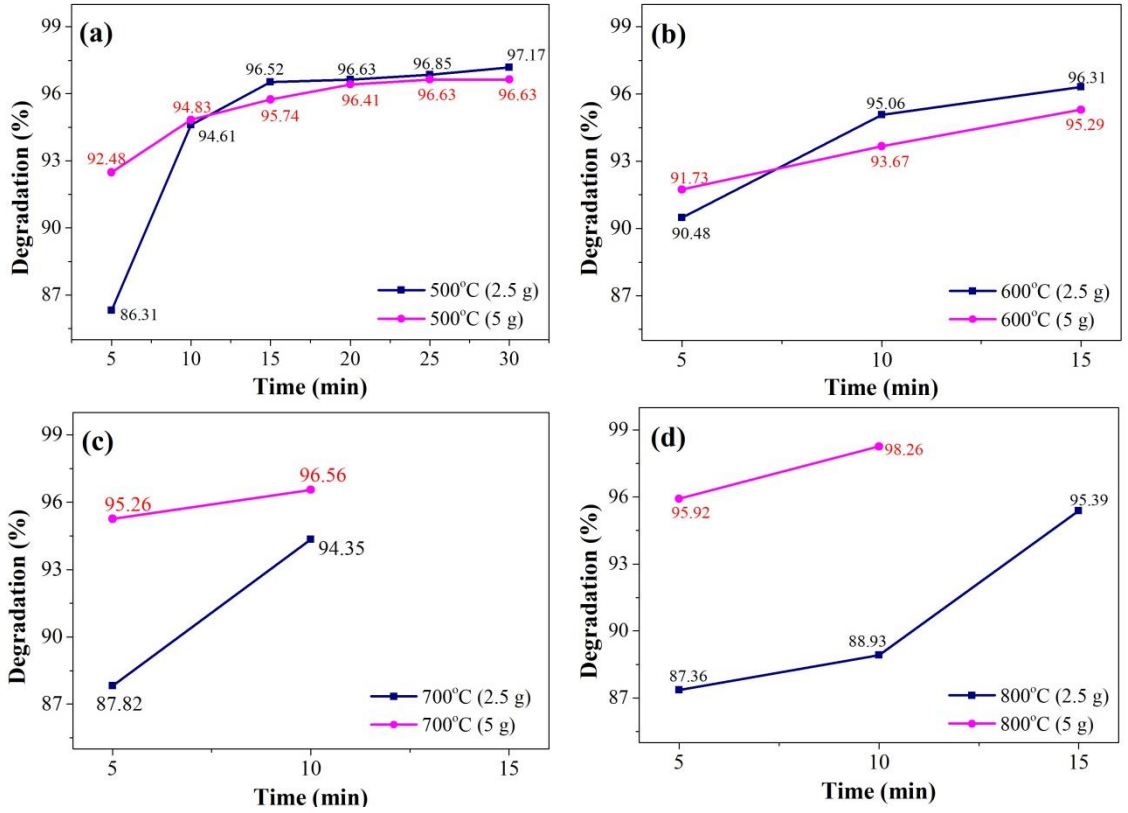

Figure 9. Percentage degradation of CR with the different catalysts (a) 500°C, (b) 600°C, (c) 700°C, and (d) 800°C

Table 3. The degradation ability of samples ZnO/TiO_2 to degrade CR with the different catalysts

Sample	Temperature (°C)	Percentage degradation (%)	Degradation time (min)
ZnO/TiO_2 (2.5 g)	500	97.17	30
	600	96.31	15
	700	94.81	10
	800	95.39	15
ZnO/TiO_2 (5 g)	500	96.63	30
	600	95.29	15
	700	96.56	10
	800	98.26	10

Figure 9 shows the kinetic model photocatalytic degradation of composites ZnO/TiO_2 for CR solution under light irradiation. Based on the kinetic model, ZnO/TiO_2 (5 g) at 800ºC shows the best material for photocatalyst with the highest photocatalytic activity. **Figure 9(c)** records the photocatalytic performance of CR degradation by using ZnO/TiO_2 (5 g) at 800ºC is faster than the other samples.

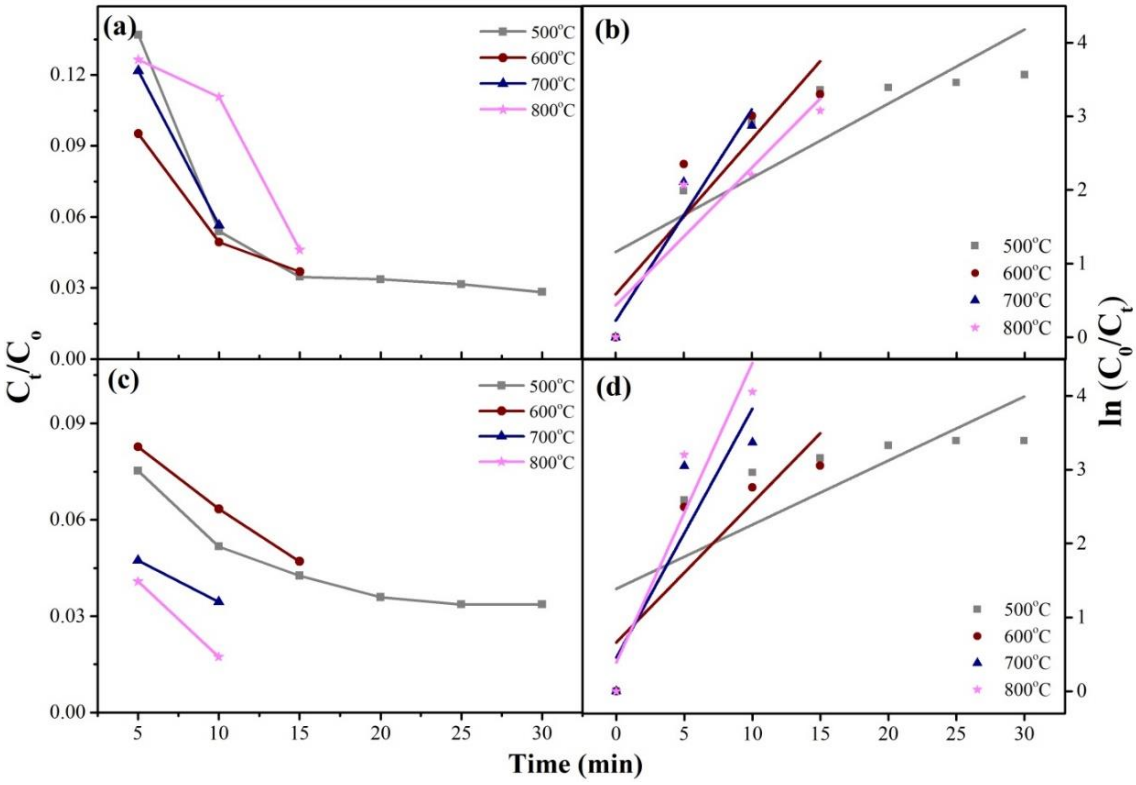

Figure 10. Photocatalytic performance and kinetic model of composites (a-b) ZnO/TiO_2 (2,5 g) and (c-d) ZnO/TiO_2 (5 g) for various calcination temperature in CR solution

Figure 10(b) and 10(d) shows the photodegradation rate kinetic curves of CR for various calcination temperature of composite materials. The degradation rate constant (k_r) in the photocatalytic reaction was calculated by the following equation [60,64]:

$$\ln \frac{C_0}{C_t} = k_r.t \qquad (14)$$

where C_0 is the initial concentration and C_t is the concentration at the time t and corresponding results for k_r and R^2 for composite ZnO/TiO_2 are shown in **Table 4**. The k_r and R^2 were increased with increasing the calcination temperature for ZnO/TiO_2 (5 g) compared to ZnO/TiO_2 (2.5 g) and the highest rate constant is for composite ZnO/TiO_2 (5 g) at 800ºC which faster degradation only for 10 min irradiation.

Table 4. Rate constants (k_r), correlation coefficient values (R^2), and band gap of ZnO/TiO_2 composites synthesized from *Calopogonium mucunoides* leaves

Sample	Temperature (ºC)	k_r (min^{-1})	R^2	Band gap (eV)
ZnO/TiO_2 (2.5 g)	500	0.11883	0.64629	3.08
	600	0.21997	0.74324	3.11
	700	0.28380	0.86531	2.89
	800	0.20506	0.78970	3.02
ZnO/TiO_2 (5 g)	500	0.11305	0.50827	3.05
	600	0.20374	0.62944	3.05
	700	0.33696	0.64080	3.05
	800	0.40521	0.79886	3.07

Photocatalytic activity

The degradation of wastewater in the photocatalytic process by demineralization of pollutant targets with final molecules are CO_2, H_2O, and N_2 [29]. During irradiation processes, there is interaction between photon with the charge particle in composite ZnO/TiO_2 at the valence band and produce electron which having energy for moving by excitation to the conduction band and remaining hole in the valence band. The heterojunction band offset link between ZnO and TiO_2 used for transfer electrons from conduction band of ZnO to conduction band of TiO_2 and transfer holes from the valence

band of TiO_2 to the valence band of ZnO [1]. By this process, the number of electrons in the conduction band of TiO_2 and the number of holes in the valence band of ZnO are increased and suppressing the recombination process. The lifetime of carrier also increases which consequently the degradation process is faster [1,29]. The schematic of degradation process of CR from the incoming photon, transfer charge (electron and hole) to the final product as shown in **Figure 11** for composite ZnO/TiO_2.

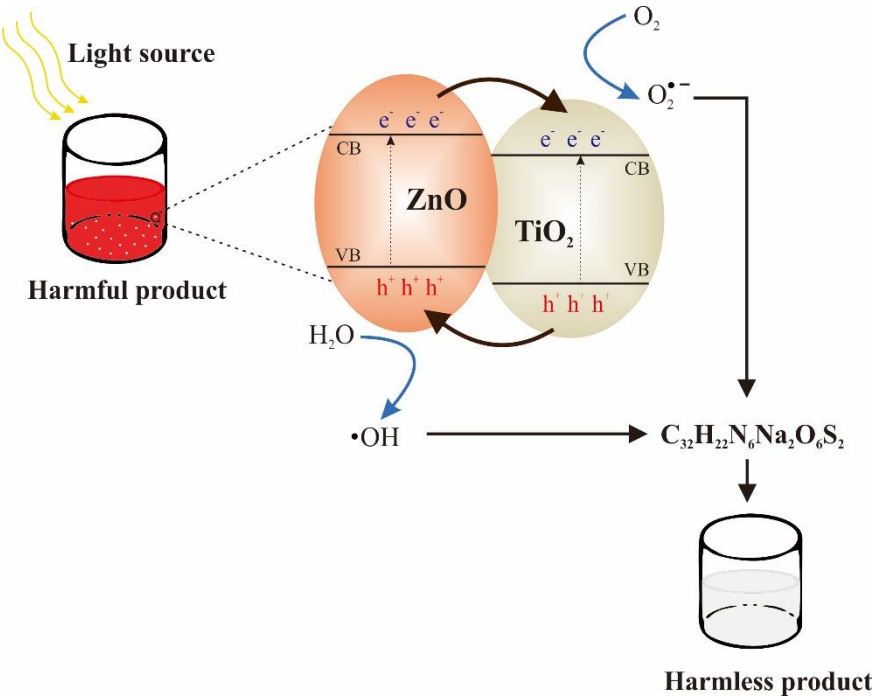

Figure 11. Schematic degradation process of CR from the incoming photon, transfer charge (electron and hole), produce radicals to break the bond of CR, and the final product of photocatalytic in the composite ZnO/TiO_2

Enhancement of electron density in conduction band of TiO_2 interacts with the surface of oxygen and it will increase superoxide radicals as products. Hole in valence band reacted with H_2O that absorbed in surface of semiconductor and the result of the reaction were hydroxyl radicals (·OH). Species of radical active such as ·OH and $\cdot O_2^-$

were used to mineralize the organic and inorganic contaminants in wastewater [1,21]. **Figure 12** shows the active radicals degraded CR dye start by the breaking the bond of molecules CR and continue with intermediates reaction to mineralize into carbon dioxide, hydrogen dioxide (water), ammonium, and nitrate ion [76].

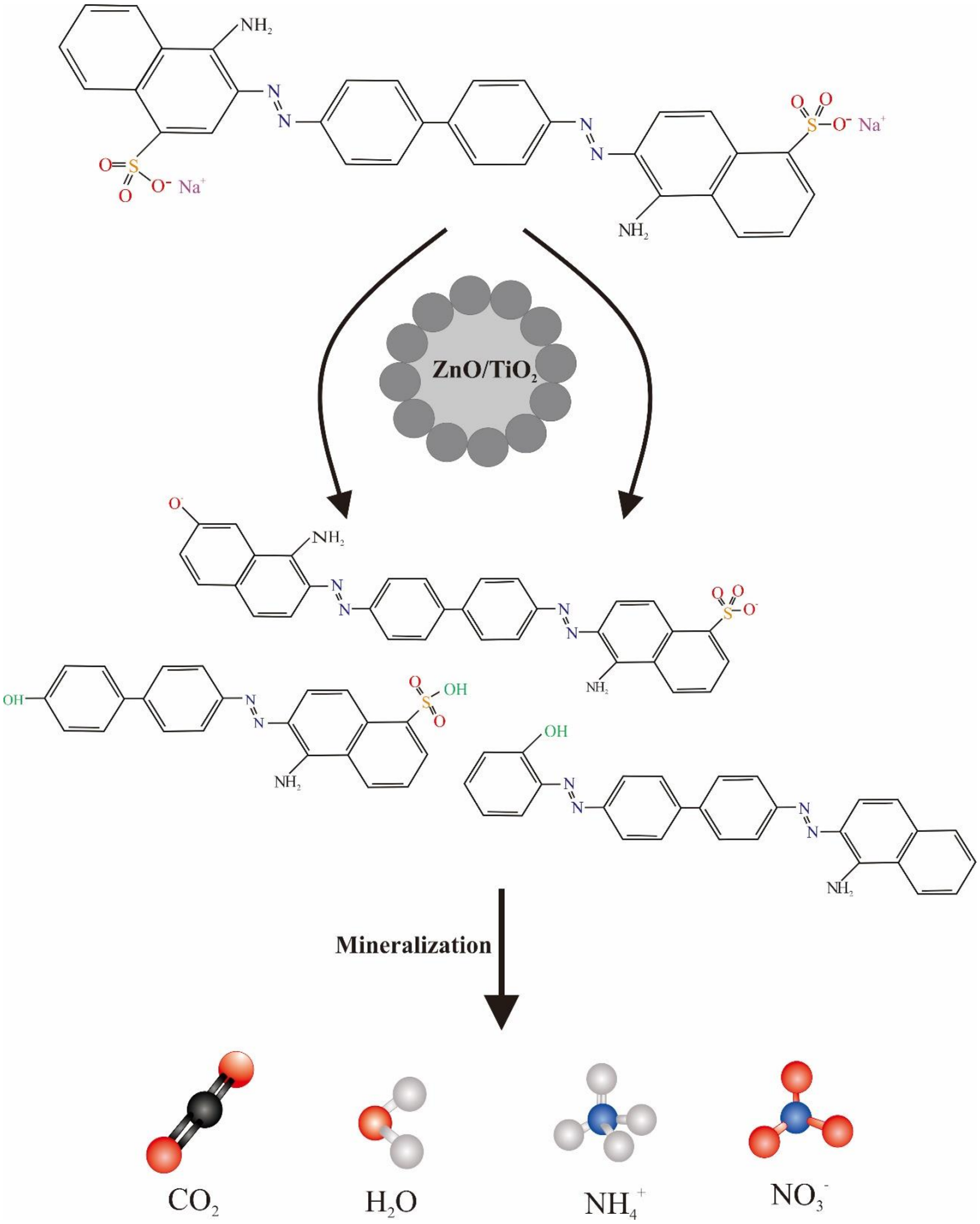

Figure 12. Demineralization mechanism of CR by the composite ZnO/TiO_2 in the photodegradation process

Recycle

In this work, five cycles successfully show the ability of composite ZnO/TiO_2 as a new and high potentials photocatalyst to be holistically integrates with environmentally friendly principles and circular chemistry, minimizing wastewater and efficiency of use the energy, water, and chemicals. **Figure 13** shows the excellent performance > 95.02% degradation of CR dye with high stability up to 5 times for every 15 min irradiation.

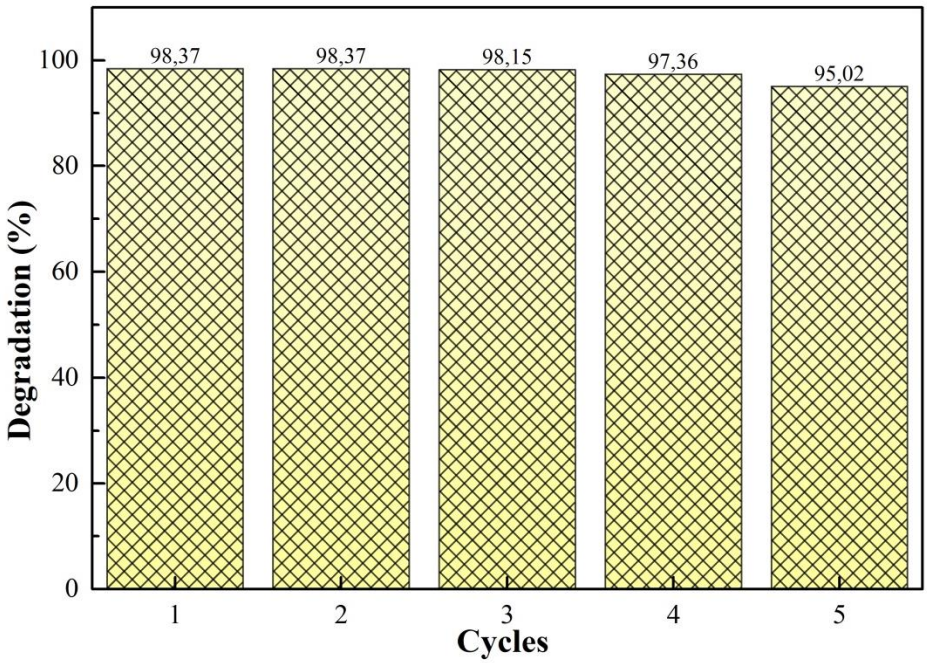

Figure 13. Stability degradation performance of composite ZnO/TiO_2 for CR dye up to five times

To show the novelty in this study, we have compared the performance of green synthesized composite ZnO/TiO_2 in this study with the previous reported references as shown in **Table 5**. The treatment time and the degradation performance in this study

shows high potentially with faster and high stability. It's indicated that the high applicability for the concept holistically integrates with environmentally friendly principles and stability for circular chemistry, minimizing wastewater and efficiency of use the energy and chemicals.

Table 5. Comparison in this study with previous reported reference of composite ZnO/TiO_2 for various synthesized methods, dye type, light sources, treatment time, and degradation performance. Clearly in this study shows faster (10 min up to30 min) with high stability (5 cycle).

Photocatalyst	**Syntesized method**	**Photocatalyst dosage**	**Dye type**	**Light source**	**Treatment time (min)**	**Degradation (%)**	**Kinetic rate (min^{-1})**	**Ref.**
$ZnO–TiO_2$ nanohybrids	Hydrothermal	0.5 g/L	MB MO OTC (60 mg/L)	Solar light (862 W)	6 (MB) 8 (OTC) 30 (R6G)	98.40 90.30 81.30	0.65172 0.27400 0.06116	[1]
ZnO/TiO_2 composite	Sol gel	0.5 g/L	Methylene blue (2 mmol/L)	UV light	360	82.00	0.2925	[14]
2-D fern-like ZnO/TiO_2	Green synthesis	0.12 g/L	Methylene blue (0.2 mg/L)	Tungsten lamp (500W)	135	98.00	0.99429	[21]
ZnO/TiO_2	Solid state	2.5 g/L	Quinoline (100 mg/L)	UV light	240	92.00	0.00560	[29]

TiO_2/ZnO composite sphere	Solvothermal	0.2 g/L	Rhodamine B (20 µmol/L)	Xenon lamp (300 W)	80	Not available	0.01400	[32]
ZnO/TiO_2 nanocomposite	Pulsed laser ablation	0.5 g/L	Methyl orange	Xenon lamp (500 W)	60	98.00	0.11420	[56]
ZnO/TiO_2 nanocomposite	Chemical method	0.5 g/L	Bentazon (20 mg/L)	UV light	120	84.20	0.01540	[62]
ZnO/TiO_2 thin film	DC reactive magnetron sputtering technique	Thin film	Methyl orange (10 mg/L)	UV light	150	91.00	Not available	[77]
ZnO/TiO_2 heterojunction	Mechanical mixing	0.5 g/L	Rhodamine B (80 mg/L)	Mercury lamp (UV light)	30	~45.00	Not available	[78]
ZnO/TiO_2 composite	Hydrothermal	Not available	MB MO (0.02 mM)	Sun light	60 (MB) 60 (MO)	Not available	0.06100 0.04700	[79]

ZnO/TiO_2	Sol gel and precipitation	0.5 g/L	Methyl orange (10^{-5} mol/L)	UV light (40W)	360	99.5	0.01760	[80]
ZnO/TiO_2 core/shell	Sol gel deposition	Thin film	Methylene blue (10 mM)	LED (140 mW, monochromatic light of 400 nm)	160	Not available	0.00700	[81]
ZnO/TiO_2 nanocomposite	Hydrothermal	A piece of composite on Ti fabric (1 cm×1 cm)/ 100 mL	Methyl orange (20 mg/L)	Xe lamp (300 W)	210	~100	Not available	[82]
ZnO/TiO_2	Electrostatically modified electrospinning	0.6 g/L	Methyl orange (3 mg/L)	UV light	360	Not available	0.01270	[83]
ZnO/TiO_2 (2.5 g)								

500ºC	Green synthesis	0.2 g/L	Congo red (40 mg/L)	Tungsten lamp (300W)	30	97.17	0.11883	Present
600 ºC	Green synthesis	0.2 g/L	Congo red (40 mg/L)	Tungsten lamp (300W)	15	96.31	0.21997	Present
700 ºC	Green synthesis	0.2 g/L	Congo red (40 mg/L)	Tungsten lamp (300W)	10	94.81	0.28380	Present
800 ºC	Green synthesis	0.2 g/L	Congo red (40 mg/L)	Tungsten lamp (300W)	15	95.39	0.20506	Present
ZnO/TiO_2 (5 g)								
500 ºC	Green synthesis	0.2 g/L	Congo red (40 mg/L)	Tungsten lamp (300W)	30	96.63	0.50827	Present
600 ºC	Green synthesis	0.2 g/L	Congo red (40 mg/L)	Tungsten lamp (300W)	15	95.29	0.62944	Present

700 °C	Green synthesis	0.2 g/L	Congo red (40 mg/L)	Tungsten lamp (300W)	10	96.56	0.64080	Present
800 °C	Green synthesis	0.2 g/L	Congo red (40 mg/L)	Tungsten lamp (300W)	10	98.26	0.79886	Present

Conclusion

The composite ZnO/TiO_2 was synthesized from *Calopogonium mucunoides* leaf extract by using green synthesis method. The composites were prepared for various calcination temperature (500ºC, 600ºC, 700ºC, and 800ºC) and different concentration of TiO_2 (2.5 g and 5 g). From XRD analysis, the crystallite size of composites was influenced by the concentration of TiO_2 and calcination temperature during the synthesis. FTIR spectra observed the Zn-O band at the peak 446 cm^{-1} and O-Ti-O band at the peak 723 cm^{-1}. The optical properties were analyzed by using K-K relation from the infra-red spectra, it shows the highest energy loss function and distance between optical phonon vibration modes (ΔLO-TO) is in the ZnO/TiO_2 (5 g) at temperature 800ºC. It indicates the stable and strong bonding formation and the lattice match in the composite which has effect to enhance photocatalytic activity. According to UV-Vis study, the synthesis of ZnO/TiO_2 shows high effectivity in photodegradation of CR dye. The materials presented the excellent photocatalytic performance with highest degradation efficiency for composite ZnO/TiO_2 (5 g) at 800ºC. In this study shows high potentially with faster and high stability, indicated that high applicability concept for holistically integrates with environmentally friendly principles and high stability for circular chemistry, and efficiency of use the energy and chemicals.

Acknowledge

This work was supported by the PT (Penelitian Terapan) funded by the Indonesia Government (Kemenristek/BRIN) grants 2021.

References

[1] J. Singh, S. Kumar, Rishikesh, A.K. Manna, R.K. Soni, Fabrication of ZnO-TiO_2 nanohybrids for rapid sunlight driven photodegradation of textile dyes and antibiotic residue molecules, Opt. Mater. 107 (2020) 110138. https://doi.org/10.1016/j.optmat.2020.110138.

[2] C.A.S. Robles, P. A. Luque, C. M. G. Gutiérrez, O. Nava, A.R.V. Nestor, E.L. Medina, R. Ranjithkumar, A.C. Beltrán, Study on the effect of the concentration of Hibiscus sabdariffa extract on the green synthesis of ZnO nanoparticles, Results in Phys. 15 (2019) 102807. https://doi.org/10.1016/j.rinp.2019.102807.

[3] S.M.T.H. Moghaddas, B. Elahi, V. Javanbakht, Biosynthesis of pure zinc oxide nanoparticles using Quince seed mucilage for photocatalytic dye degradation, J. Alloys Compd. 821 (2020) 153519. https://doi.org/10.1016/j.jallcom.2019.153519.

[4] M.M. Ghoneim, H.S. El-Desoky, N.M. Zidan, Electro-Fenton oxidation of sunset yellow FCF azo-dye in aqueous solutions, Desalination 274 (1-3) (2011) 22-30. https://doi.org/10.1016/j.desal.2011.01.062.

[5] M.B. Shekardasht, M.H. Givianrad, P.Gharbani, Z. Mirjafary, A. Mehrizad, Preparation of a novel Z-scheme g-C_3N_4/RGO/$Bi_2Fe_4O_9$ nanophotocatalyst for degradation of congo red dye under visible light, Diamond & Related Mater. 109 (2020) 108008. https://doi.org/10.1016/j.diamond.2020.108008.

[6] X. Wang, B. Deng, L. Yu, E. Cui, Z. Xiang, W. Lu, Degradation of azo dyes congo red by MnBi alloy powders: performance, kinetics and mechanism, Mater. Chem. Phys. 251 (2020) 123096. https://doi.org/10.1016/j.matchemphys.2020.123096.

[7] M.M. Tauber, G.M. Gübitz, A.Rehorek, Degradation of azo dye by oxidation processes-laccase and ultrasound treatment, Bioresource Technol. 99 (10) (2008) 4213-4220. https://doi.org/10.1016/j.biortech.2007.08.085.

[8] Y.P. Feng, N. Gaztelumendi, J. Fornell, H.Y. Zhang, P. Solsona, M.D. Baro, S. Surinach, E. Ibanez, L. Barrios, E. Pellicer, C. Nogues, J. Sort, Mechanical properties, corrosion performance, and cell viability studies on newly developed porous Fe-Mn-Si-Pd alloy, J. Alloys Compd. 724 (2017) 1046-1056. https://doi.org/10.1016/j.jallcom.2017.07.112.

[9] S.A. Bhat, F. Zafar, A.H. Mondal, A. Kareem, A.U. Mirza, S. Khan, A. Mohammad, Q.M.R. Haq, N. Nishat, Photocatalytic degradation of carcinogenic congo red dye in aqueous solution, antioxidant activity and bactericidal effect of NiO nanoparticles, J. Iran. Chem. Soc. 17 (1) (2020) 215-227. https://doi.org/10.1007/s13738-019-01767-3.

[10] A.R. Binupriya, M. Sathishkumar, K. Swaminathan, C.S. Kuz, S.E. Yun, Comparative studies on removal of congo red by native and modified mycelial pellets of trametes versicolor in various reactor modes, Bioresource Technol. 99 (5) (2008) 1080–1088. https://doi.org/10.1016/j.biortech.2007.02.022.

[11] D. Tekin, H. Kiziltas, H. Ungan, Kinetic evaluation of ZnO/TiO_2 thin film photocatalyst in photocatalytic degradation of Orange G, J. Molec. Liquids 306 (2020) 112905. https://doi.org/10.1016/j.molliq.2020.112905.

[12] M. Kazemaini, M. Nikkhah, M. Fattahi, L. Vafajoo, Physiochemical properties and catalytic performances of nanostructured V_2O_5 over TiO_2 and γ-Al_2O_3 for oxidative dehydrogenation of propane, Chem. Biochem. Eng. Q. 30 (2016) 9-18. https://doi.org/10.15255/CABEQ.2014.2049.

[13] A.H. Zyoud, A. Zubi, S. Hejjawi, S.H. Zyoud, M.H. Helal, S.H. Zyoud, N. Qamhiehe, A.R. Hajamohideen, H.S. Hilal, Removal of acetaminophen from water by simulated solar light photodegradation with ZnO and TiO2 nanoparticles: Catalytic efficiency assessment for future prospects, J. Environ. Chem. Eng. 8 (2020) 104038. https://doi.org/10.1016/j.jece.2020.104038.

[14] L. Munguti, F. Dejene, Influence of annealing temperature on structural, optical, and photocatalytic properties of ZnO-TiO_2 composites for application in dye removal in water, Nano-Struct. Nano-Objects 24 (2020) 100594. https://doi.org/10.1016/j.nanoso.2020.100594.

[15] K.M. Lee, C.W. Lai, K.S. Ngai, J.C. Juan, Recent development of zinc oxide based photocatalyst in water treatment technology: A review, Water Res. 88 (2016) 428-448. https://doi.org/10.1016/j.watres.2015.09.045.

[16] G. Madhumitha, J. Fowsiya, N. Gupta, A. Kumar, M. Singh, Green synthesis, characterization and antifungal and photocatalytic activity of Pithecellobium dulce peel mediated ZnO nanoparticles, J. Phys. Chem. Solids 127 (2019) 43-51. https://doi.org/10.1016/j.jpcs.2018.12.005.

[17] N.T. Hanh, N.L.M. Tri, D.V. Thuan, M.H.T. Tung, T.D. Pham, T.D. Minh, H.T. Trang, M.T. Binh, M.V. Nguyen, Monocrotophos pesticide effectively removed by novel visible light driven Cu doped ZnO photocatalyst, J. Photochem. Photobiol. A.: Chem. 382 (2019) 111923. https://doi.org/10.1016/j.jphotochem.2019.111923.

[18] H. Bouzid, M. Faisal, F.A. Harraz, S.A. AL-Sayari, A.A. Ismail, Synthesis of mesoporous Ag/ZnO catalyst and photocatalyst activity, Catal. Today 252 (2015) 20-26. https://doi.org/10.1016/j.cattod.2014.10.011.

[19] N.T. Truc, D.T. Tran, N.T. Hanh, T.D. Pham, Novel visible light-driven Nb-Doped Ta_3N_5 sensitized/protected by PPy for efficient overall water splitting, Int. J. Hydrogen Energy 43 (2018) 5480-5495. https://doi.org/10.1016/j.ijhydene.2018.06.128.

[20] M.R.D. Khaki, M.S. Shafeeyan, A.A.A. Raman, W.M.A W. Daud, Enhanced UV-Visible photocatalytic activity of Cu-doped ZnO/TiO_2 nanoparticles, J. Mater. Sci. Mater. Electron. 29 (2018) 5480-5495. https://doi.org/10.1007/s10854-017-8515-9.

[21] N. Suganthi, S. Thangavel, K. Kannan, Hibiscus subdariffa leaf extract mediated 2-D fern-like ZnO/TiO2 hierarchical nanoleaf for photocatalytic degradation, FlatChem 24 (2020) 100197. https://doi.org/10.1016/j.flatc.2020.100197.

[22] M.S.H. Bhuiyan, M.Y. Miah, S.C. Paul, T.D. Aka, O. Saha, M.M. Rahaman, M.J.I. Sharif, O. Habiba, M. Ashaduzzaman, Green synthesis of iron oxide nanoparticle using Carica papaya leaf extract: application for photocatalytic degradation of remazol yellow RR dye and antibacterial activity, Heliyon 6 (2020) e04603. https://doi.org/10.1016/j.heliyon.2020.e04603.

[23] H. Kamani, S. Nasseri, M. Khoobi, R.N. Nodehi, A.H. Mahvi, Sonocatalytic degradation of humic acid by N-doped TiO_2 nano-particle in aqueous solution, J.Environ. Health Sci. Eng. 14 (2016) 3. https://doi.org/10.1186/s40201-016-0242-2.

[24] R. Ashouri, P. Ghasemipoor, B. Rasekh, F. Yazdin, S. Mofradnia, The effect of ZnO-based carbonaceous materials for degradation of benzoic pollutants: a review, Int. J. Environ. Sci. Technol. 16 (2019) 1729-1740. https://doi.org/10.1007/s13762-018-2056-5.

[25] M.H. Malakooti, H.S. Hwang, H.A. Sodano, Morphology-controlled ZnO nanowire array for tailored hybrid composites with high damping, ACS Appl. Mater. Interfaces 7 (2014) 332-339. https://doi.org/10.1021/am506272c.

[26] H. Fang, Y. Guo, T. Wu, Y. Liu, Biomimetic synthesis of urchin-like CuO/ZnO nanocomposites with excellent photocatalytic activity, New J. Chem. 42 (2018) 12779-12786. https://doi.org/10.1039/C8NJ02052C.

[27] S. Ma, J. Xue, Y. Zhou, Z. Zhang, Photochemical synthesis of ZnO/Ag_2O heterostructures with enhanced ultaviolet and visible photocatalytic activity, J. Mater. Chem. A. 2 (2014) 7272-7280. https://doi.org/10.1039/C4TA00464G.

[28] D. Ma, J. W. Shi, Y. Zou, Z. Fan, X. Ji, C. Niu, Highly efficient photocatalyst based on CdS quantum dots/ZnO nanosheets 0D/2D heterojunction for hydrogen evolution from water splitting, ACS Appl. Mater. Interfaces 9 (2017) 25377-25386. https://doi.org/10.1021/acsami.7b08407.

[29] D. Gupta, R. Chauhan, N. Kumar, V. Singha, V.C. Srivastava, P. Mohanty, T.K. Mandal, Enhancing photocatalytic degradation of quinoline by ZnO:TiO2 mixed oxide: Optimization of operating parameters and mechanistic study, J. Environ. Management 258 (2020) 110032. https://doi.org/10.1016/j.jenvman.2019.110032.

[30] K.S. Stefaríska, A. Kubiak, A. Piasecki, J. Goscianska, G. Nowaczyk, S. Jurga, T. Jesionowski, TiO_2-ZnO binary oxide systems: comprehensive characterization and tests of photocatalytic activity, Materials 11 (2018) 841. https://doi.org/10.3390/ma11050841.

[31] C. Cheng, A. Amini, C. Zhu, Z. Xu, H. Song, N. Wang, Enhanced photocatalytic performance of TiO_2-ZnO hybrid nanostructures, Sci. Rep. 4 (2014) 4181. https://doi.org/10.1038/srep04181.

[32] L. Pan, G.Q. Shen, J.W. Zhang, X.C. Wei, L.Wang, J.J. Zou, X. Zhang, TiO_2-ZnO composite sphere decorated with ZnO clusters for effective charge isolation in photocatalysis, Indus. Eng. Chem. Res. 54 (2015) 7226-7232. https://doi.org/10.1021/acs.iecr.5b01471.

[33] M.Y. Guo, M.K. Fung, F. Fang, X.Y. Chen, A.M.C. Ng, A.B. Djurišić, W.K. Chan, ZnO and TiO_2 1D nanostructures for photocatalytic applications, J. Alloys Compd. 509 (2011) 1328-1332. https://doi.org/10.1016/j.jallcom.2010.10.028.

[34] M. Hosseini, A. Haghighatzadeh, Bmazinani, Enhanced third-order optical susceptibility in heterogeneous wurtzite ZnO/ anatase TiO_2 core/ shell nanostructures via controlled TiO_2 shell thickness, Opt. Mater. 92 (2019) 1-10. https://doi.org/10.1016/j.optmat.2019.03.042.

[35] G.K. Upadhyay, J.K. Rajput, T.K. Pathak, V. Kumar, L.P. Purohit, Synthesis of zno:tio_2 nanocomposites for photocatalyst application in visible light, Vacuum 160 (2019) 154-163. https://doi.org/10.1016/j.vacuum.2018.11.026.

[36] F.A.M. Al-Zahrani, R.M. El-Shishtawy, N.S.E. Ahmed, N.S. Awwad, M.S. Hamdy. A.M. Asiri, Photocatalytic decolourization of a new water-insoluble organic dye based on phenothiazine by ZnO and TiO_2 nanoparticles, Arabian J. Chem. 13 (2020) 3633-3638. https://doi.org/10.1016/j.arabjc.2019.12.007.

[37] H. Wang, L. Zhang, L. Chen, J. Hu, S. Li, Z. Wang, J. Liu, X. Wang, Semiconductor heterojunction photocatalysts: design, construction, and photocatalytic performances, Chem. Soc. Rev. 24 (2014) 5234-5244. https://doi.org/10.1039/C4CS00126E.

[38] S. Deebansok, T. Amornsakchai, P. Sae-ear, P. Siriphannon, S. M. Smith, Sphere-like and flake-like ZnO immobilized on pineapple leaf fibers as easy-to-recover

photocatalyst for the degradation of congo red, J. Environ. Chem. Eng. 9 (2020) 104746. https://doi.org/10.1016/j.jece.2020.104746.

[39] U.O. Bhagwat, J.J. Wu, A.M. Asiri, S. Anandan, Sonochemical Synthesis of Mg-TiO_2 nanoparticles for persistent congo red dye degradation, J. Photochem. Photobiol. A. 346 (2017) 559-569. https://doi.org/10.1016/j.jphotochem.2017.06.043.

[40] P.S. Basavarajappa, S.B. Patil, N. Ganganagappa, K.R. Reddy, A.V. Raghu, C.V. Reddy, Recent progress in metal-doped TiO_2, non-nanometal doped/codoped TiO_2 and TiO_2 nanostructured hybrids for enhanced photocatalysis, International J. Hydrogen Energy 45 (13) (2020) 7764-7778. https://doi.org/10.1016/j.ijhydene.2019.07.241.

[41] S. Feizpoor, A.H. Yangjeh, K. Yubuta, Integration of carbon dots and polyaniline with TiO_2 nanoparticles: substantially enhanced photocatalytic activity to removal various pollutants under visible light, J. Photochem. Photobiol. A. 367 (2018) 94-104. https://doi.org/10.1016/j.jphotochem.2018.08.017.

[42] K.R. Reddy, K.V. Karthik, S.B.B. Prasad, S.K. Soni, H.M. Jeong, A.V. Raghu, Enhanced photocatalytic activity of nanostructured titanium dioxide/polyaniline hybrid photocatalyst, Polyhedron 120 (2016) 169-174. https://doi.org/10.1016/j.poly.2016.08.029.

[43] J.F. de Lima, M.H. Harunsani, D.J. Martin, D. Kong, P.W. Dunne, D. Gianolio, R.J. Kashtiban, J. Sloan, O.A. Serra, J. Tang, R.I. Walton, Control of chemical state of cerium in doped anatase TiO_2 by solvothermal synthesis and its application in photocatalytic water reduction, J. Mater. Chem. A. 3 (2015) 9890-9898. https://doi.org/10.1039/C5TA01474C.

[44] G.S. Guo, C.N. He, Z.H. Wang, F.B. Gu, D.M. Han, Synthesis of titania and titanate nanomaterials and their application in environmental analytical chemistry, Talanta 72 (2007) 1687-1692. https://doi.org/10.1016/j.talanta.2007.03.039.

[45] A.Z.Y. Qu, S. Ali, N. Sun, H. Lu, R. Yan, X. Zhang, L. Jing, Improved visible-light activities for degrading pollutants on TiO_2/g-C_3N_4 nanocomposites by decorating SPR Au nanoparticles and 2,4-dichlorophenol decomposition path, J. Hazard. Mater. 342 (2018) 715-723. https://doi.org/10.1016/j.jhazmat.2017.09.005.

[46] J. Zhou, G. Tian, Y. Chen, J. Wang, X. Cao, Y. Shi, K. Pan, H. Fu, Synthesis of hierarchical TiO_2 nanoflower with anatase-rutile heterojunvtion as Ag support for efficient visible-light photocatalytic activity, Dalton Trans. 42 (2013) 11242-11251. https://doi.org/10.1039/C3DT51293B.

[47] C. Vidya, C. Manjunatha, M.N. Chandraprabha, M. Rajshekar, M. A. L. A. Raj, Hazard free green synthesis of ZnO nano-photo-catalyst using Artocarpus Heterophyllus leaf extract for the degradation of congo red dye in water treatment applications, J. Environ. Chem. Eng. 5 (2017) 3172-3180. http://dx.doi.org/10.1016/j.jece.2017.05.058.

[48] S.P. Goutam, G. Saxena, V. Singh, A.K. Yadav, R.N. Bharagava, K.B. Thapa, Green synthesis of TiO_2 nanoparticles using leaf extracts of Jatropha curcas L for photocatalytic degradation of tannery wastewater, Chem. Eng. J. 335 (2018) 386-396. https://doi.org/10.1016/j.cej.2017.12.029.

[49] P.A. Luquea, O. Navaa, C.A. Soto-Roblesa, M.J. Chinchillas-Chinchillasa, H.E. Garrafa-Galvezb, Y.A. Baez-Lopeza, K.P. Valdez-Núñezc, A.R. Vilchis-Nestord, A. Castro-Beltránb, Improved photocatalytic efficiency of SnO_2 nanoparticles

through green synthesis, Opt. Int. J. Light and Electron Optics 206 (2020) 164299. https://doi.org/10.1016/j.ijleo.2020.164299.

[50] S. Yedurkar, C. Maurya, P. Mahanwar, Biosynthesis of zinc oxide nanoparticles using Coccinea leaf extract –a green approach, Open Journal of Synthesis and Applications 5 (2016) 1-14. http://dx.doi.org/10.4236/ojsta.2016.51001.

[51] D. Wu, C. Li, Q. Kong, S. Zaifeng, D. Zhang, L. Wang, L. Han, X. Zhang, Q. Lin, Photocatalytic activity of Lu^{3+}/TiO_2 prepared by ball milling method, Journal of Rare Earths 8 (36) (2018) 819-825. https://doi.org/10.1016/j.jre.2018.01.016.

[52] S. Ilyas, Heryanto, B. Abdullah, D. Tahir, X-ray diffraction analysis of nanocomposite Fe_3O_4/activated carbon by Williamson–Hall and size-strain plot methods, Nano-Struct. Nano-Objects 20 (2019) 100396. https://doi.org/10.1016/j.nanoso.2019.100396.

[53] B. Abdullah, S. Ilyas, D. Tahir, Nanocomposites Fe/Activated Carbon/PVA for Microwave Absorber: Synthesis and Characterization, J. Nanomater. 2018 (2018) 9823263. https://doi.org/10.1155/2018/9823263.

[54] Heryanto, Hendri, B. Abdullah, D. Tahir, Analysis of structural properties of X-ray diffraction for composite copper-activated carbon by modified Williamson-Hall and size-strain plotting methods, J. Phys.: Conf. Ser. 1080 (1) (2018) 012007. https://doi.org/10.1088/1742-6596/1080/1/012007.

[55] I. Choudhary, R. Shukla, A. Sharma, K Raina, Effect of excitation wavelength ang europium doping on the optical properties of nanoscale zinc oxide, J. Mater. Sci.: Mater. Electron. 31 (2020) 20033-20042. https://doi.org/10.1007/s10854-020-04525-x.

[56] M.A. Gondal, A.M. Ilyas, U. Baig, Pulsed laser ablation in iquid synthesis of ZnO/TiO_2 nanocomposite catalyst with enhanced photovoltaic and photocatalytic performance, Ceramic International 42 (2016) 13151-13160. https://doi.org/10.1016/j.ceramint.2016.05.104.

[57] M. Jose, M. Elakiya, S.A.M.B. Dhas, Structural and optical properties of nanosized $ZnO/ZnTiO_3$ composite materials synthesized by a facile hydrothermal technique, J. Mater. Sci.: Mater. Electron. 28 (2017) 13649-13658. https://doi.org/10.1007/s10854-017-7207-9.

[58] Y.C. Liang, C.Y. Hu, Y.C. Liang, Crystallographic phase evolution of ternary Zn-Ti-O nanomaterials during high temperature annealing of $ZnO-TiO_2$ nanocomposites, CrystEngComm 14 (2012) 5579-5584. https://doi.org/10.1039/C2CE25347J.

[59] S. Mathur, M. Arya, R. Jain, S.K. Sharma, Effect of annealing temperature on structural, electrical, and optical properties of TiO_2 nanopowder, J. Nanostruct. 7 (2) (2017) 121-126. https://dx.doi.org/10.22052/jns.2017.02.005.

[60] S. Ilyas, B. Abdullah, D. Tahir, Enhancement of absorbing frequency and photo-catalytic performance by temperature treatment of composites Fe_3O_4-AC naniparticle, Adv. Powder Technol. 31 (2020) 905-913. https://doi.org/10.1016/j.apt.2019.11.007.

[61] B. Ulum, S. Ilyas, A.N. Fahri, I. Mutmainna, M.A. Anugrah, N. Yudasari, E.B. Demmalino, D. Tahir, Composite carbon-lignin/ zinc oxide nanocrystalline ball-like hexagonal mediated from Jatropha curcas L leaf as photocatalyst for industrial dye degradation, J. Inorg. Organomet. Polym. Mater. 30 (12) (2020) 4905-4916. https://doi.org/10.1007/s10904-020-01631-5.

[62] M. Gholami, M.S. Siboni, M. Farzadkia, J.K. Yang, Synthesis, characterization, and application of ZnO/TiO_2 nanocomposite for photocatalysis of a herbicide (Bentazon), Desalination and Water Treatment 57 (29) (2016) 13632-13644. https://doi.org/10.1080/19443994.2015.1060541.

[63] S. Bagheri, K. Shameli, S.B.A. Hamid, Synthesis and characterization of anatase titanium dioxide nanoparticles using egg white solution via sol-gel method, J. Chem. 2013 (2013) 848205. https://doi.org/10.1155/2013/848205.

[64] N. Rauf, S. Ilyas, H. Heryanto, R. Rahmat, A. N. Fahri, M.H. Rahmi, D. Tahir, The correlation between structural and optical properties of zinc hydroxide nanoparticle in supports photocatalytic performance, Opt. Mater. 112 (2021) 110780. https://doi.org/10.1016/j.optmat.2020.110780.

[65] S. Suryani, H. Heryanto, R. Rusdaeni, A.N. Fahri, D. Tahir, Quantitative analysis of diffraction and infra-red spectra of composite cement/$BaSO_4$/Fe_3O_4 for determining correlation between attenuation coefficient, structural, and optical properties, Ceramic International 46 (2020) 18601-18607. https://doi.org/10.1016/j.ceramint.2020.04.170.

[66] D. Tahir, S.K. Oh, H.J. Kang, S. Tougaard, Quantitative analysis of reflection electron energy loss spectra to determine electronic and optical properties of Fe-Ni alloy thin films, J. Electron. Spectrosc. Relat. Phenom. 206 (2016) 6–11. https://doi.org/10.1016/j.elspec.2015.11.005.

[67] D. Tahir, S. Tougaard, Electronic and optical properties of selected polymers studied by reflection electron energy loss spectroscopy, J. Appl. Phys. 111 (2012) 054101. https://doi.org/10.1063/1.3688327.

[68] G.H. Khorrami, A.K. Zak, A. Kompany, R. Yousefi, Optical and Structural properties of X-doped (X=Mn, Mg, and Zn) PZT nanoparticle by Kramers-Kronig and size strain plot methods, Ceramic International 38 (2002) 5683-5690. https://doi.org/10.1016/j.ceramint.2012.04.012.

[69] Y. Yang, S. He, Y. Ye, X. Cao, H. Liu, Z. Wu, J. Yue, H. Sue, Enhanced hydrophobicity of soybean protein isolate by low-pH shifting treatment fot the sub-micron gel particles praparation, Ind. Crop. Prod. 151 (2020) 113709. https://doi.org/10.1016/j.indcrop.2020.112475.

[70] M. Ghasemifard, E. Fathi, M. Ghamari, The effect of Fe^{3+}-doped on structure and optical properties of mesoporous Al_2O_3/SiO_2 composite, Mater. Sci. Semicond. Process. 42 (2016) 349–353. https://doi.org/10.1016/j.mssp.2015.11.001.

[71] X. Lu, J. Chen, M. Zheng, J. Guo, J. Qi, Y. Chen, S. Miao, B. Zheng, Effect of highintensity ultrasound irradiation on the stability and structural features of coconutgrain milk composite system utilizing maize kernels and starch with different amylose contents, Ultrason. Sonochem. 55 (2019) 135–148. https://doi.org/10.1016/j.ultsonch.2019.03.003.

[72] D. Tahir, S.K. Oh, H.J. Kang, S. Tougaard, Composition dependence of dielectric and optical properties of Hf-Zr-silicate thin films grown on Si (100) by atomic layer deposition, Thin Solid Films 116 (2016) 425–430. https://doi.org/10.1016/j.tsf.2016.09.001.

[73] D. Tahir, Suarga, N.H. Sari, Yulianti, Stopping powers and inelastic mean free path of 200 eV–50 keV electrons in polymer PMMA, PE, and PVC, Applied Radiation and Isotopes 95 (2015) 59-62. https://doi.org/10.1016/j.apradiso.2014.10.001.

[74] S. Mugundan, B. Rajamman, G. Viruthagiri, N. Shanmugam, R. Gobi, P. Praveen, Synthesis and characterization of undope and cobalt-doped TiO_2 nanoparticles via sol-gel technique. Appl. Nanosci. 5 (2015) 449-456. https://doi.org/10.1007/s13204-014-0337-y.

[75] N. Selvi, S. Sankar, K. Dinakaran, Effect of shell ZnO on the structure and optical property of TiO_2 core@shell hybrid nanoparticles, J. Mater. Sci.: Mater. Electron. 26 (2015) 2271-2277. https://doi.org/10.1007/s10854-015-2680-5.

[76] M. Thomas, G.A. Naikoo, M.U.D. Sheikh, M. Bano, F. Khan, Effective photocatalytic degradation of congo red dye using alginate/carboxymethyl cellulose/TiO_2 nanocomposite hydrogel under direct sunlight irradiation, J. Photochem. Photobiol. A. 327 (2016) 33-43. https://doi.org/10.1016/j.jphotochem.2016.05.005.

[77] N.Q.T. Ton, T.N.T. Le, S. Kim, V.A. Dao, J. Yi, T.H.T. Vu, High-efficiency photo-generated charges of ZnO/TiO_2 heterojunction thin films for photocatalytic and antibacterial performance, J. Nanosci. Nanotechnol. 20 (2020) 2214-2222. https://doi.org/10.1166/jnn.2020.17306.

[78] W. Sun, S. Meng, S. Zhang, X. Zheng, X. Ye, X. Fu, S. Chen, Insight into the tranfer mechanisms of photogenerated carriers for heterojunction photoocatalyst with analogous position of valence band and conduction band: a case study of ZnO/TiO_2, J. Phys. Chem. C. 122 (27) (2018) 15409-15420. https://doi.org/10.1021/acs.jpcc.8b03753.

[79] A. Das, P.M. Kumar, M. Bhagavathiachari, R.G. Nair, Hierarchical ZnO-TiO_2 nanoheterojunction: a strategy driven approach to boost the photocatalytic performance through the synergy of improved surface area and interfacial charge

transport, Appl. Surface Sci. 534 (2020) 147321. https://doi.org/10.1016/j.apsusc.2020.147321.

[80] A.E. Mragui, I. Daou, O. Zegaoui, Influence of the preparation method and ZnO/(ZnO+TiO_2) weight ratio on the physicochemical and photocatalytic properties of ZnO-TiO_2 nanomaterials, Catal. Today 321 (2019) 41-51. https://doi.org/10.1016/j.cattod.2018.01.016.

[81] M. Kwiatkowski, R. Chassagnon, O. Heintz, N. Geoffroy, M. Skompska, I. Bezverkhyy, Improvement of photocatalytic and photoelectrochemical activity of ZnO/TiO_2 core/shell system through additional calcination: insight into the mechanism, Appl. Catal. B: Environ. 204 (2017) 200-208. https://doi.org/10.1016/j.apcatb.2016.11.030.

[82] C. Wang, X. Li, N. Xia, M. Jiang, R. Liu, J. Huang, Q. Li, Z. Luo, L. Liu, W. Xu, D. Fan, Novel ZnO-TiO_2 nanocomposite arrays on Ti fabric for enhanced photocatalytic application, J. Molec. Struct. 1148 (2017) 347-355. https://doi.org/10.1016/j.molstruc.2017.07.030.

[83] P.G. Ramos, E. Flores, L.A. S´anchez, R.J. Candal, M. Hojamberdiev, W. Estrada, J. Rodriguez, Enhanced photoelectrochemical performance and photocatalytic activity of ZnO/TiO_2 nanostructures fabricated by an electrostatically modified electrospinning, Appl. Surface Sci. 426 (2017) 844-851. https://doi.org/10.1016/j.apsusc.2017.07.218.

Figures

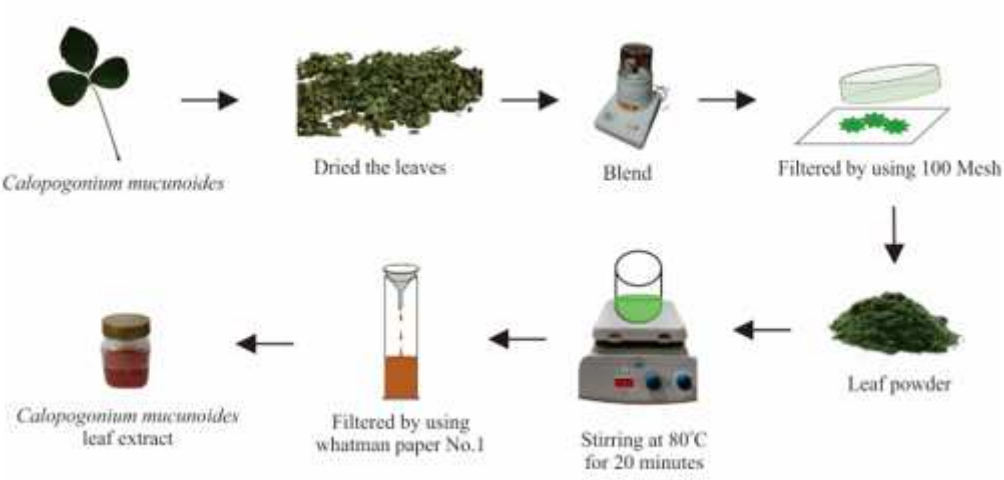

Figure 1

Schematic illustration for extraction of Calopogonium mucunoides leaves

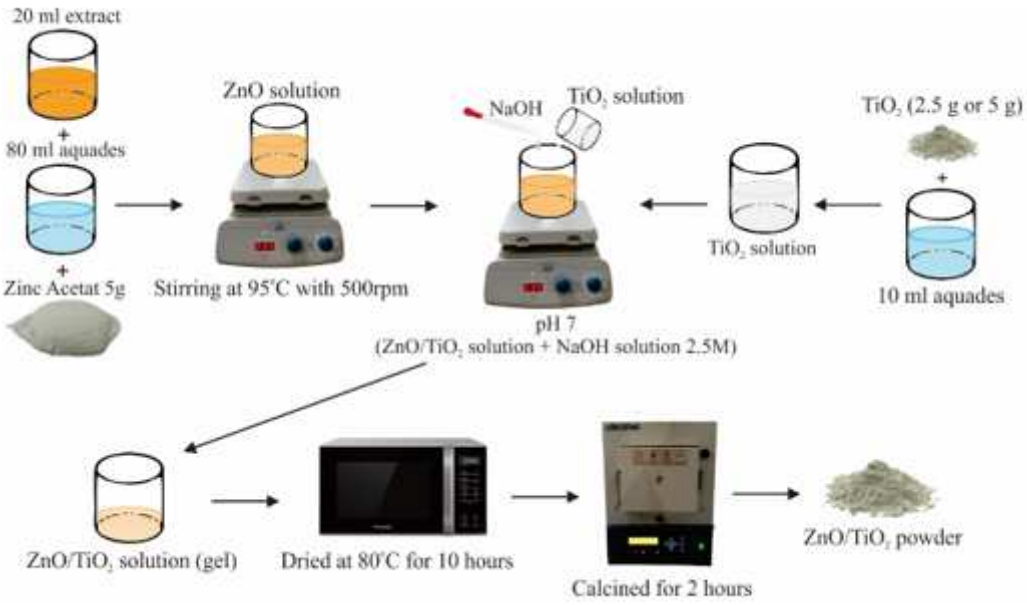

Figure 2

Illustration procedure of green synthesis ZnO/TiO2 using Calopogonium mucunoides leaf extract

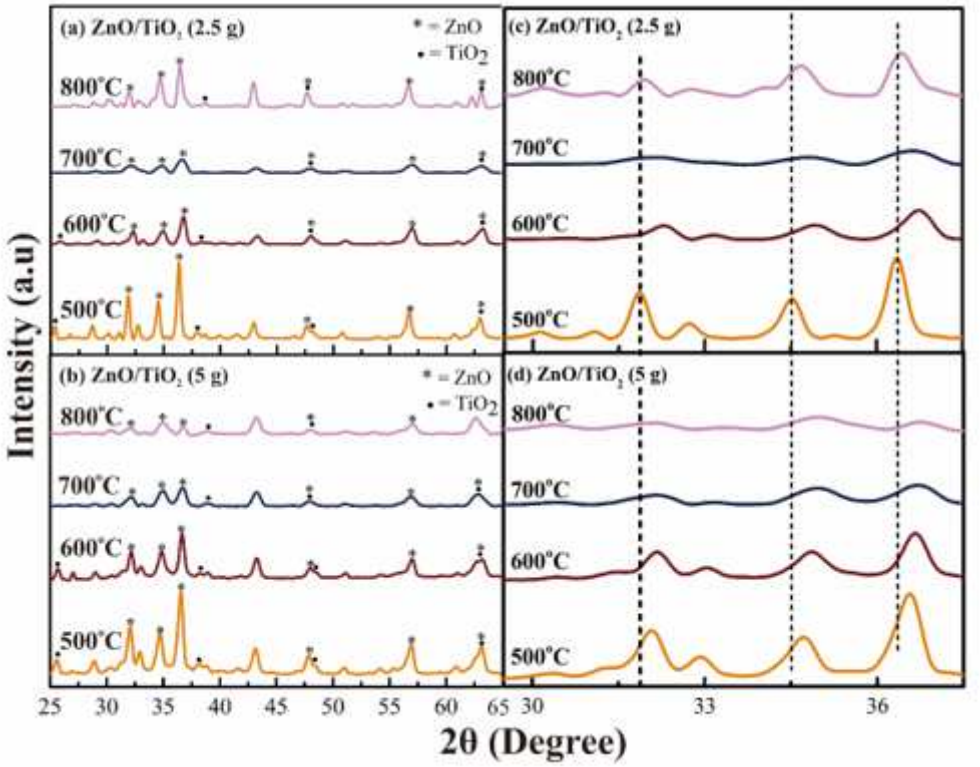

Figure 3

XRD analysis of ZnO/TiO2 synthesized from Calopogonium mucunoides leaves extract for various calcination temperature (500oC, 600oC, 700oC, 800oC) and TiO2 concentration (2.5 g and 5 g)

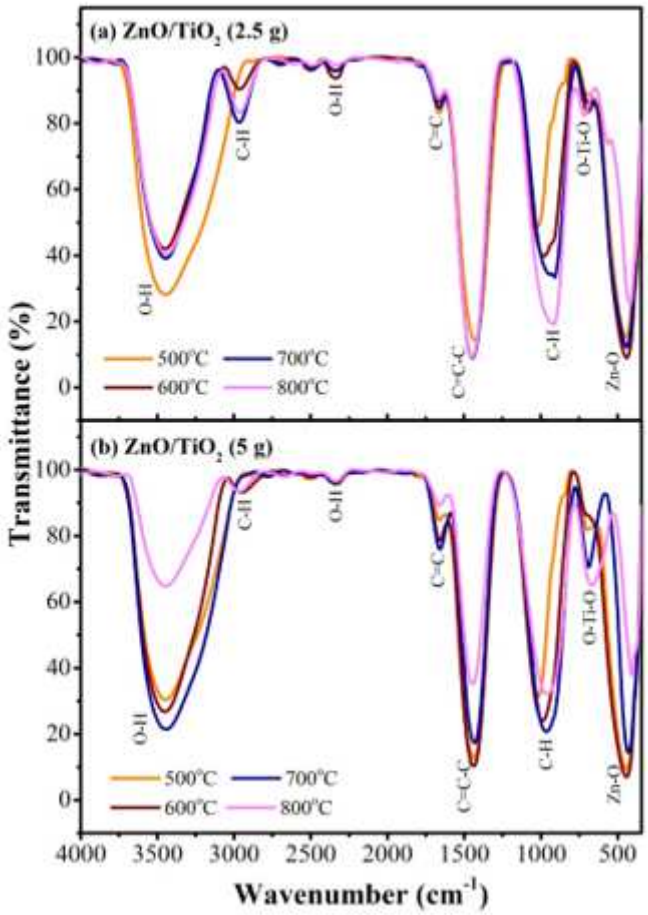

Figure 4

FTIR spectra of ZnO/TiO2 synthesized from Calopogonium mucunoides leaves extract for various calcination temperature (500oC, 600oC, 700oC, 800oC) and TiO2 concentration (2.5 g and 5 g)

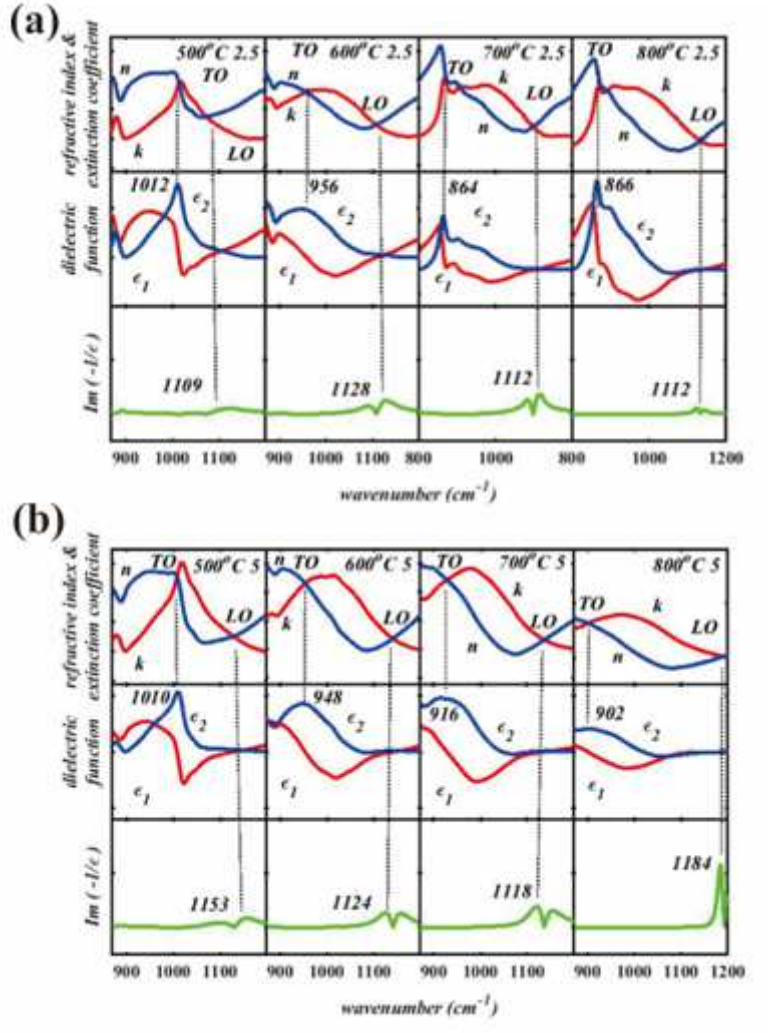

Figure 5

The optical properties (refractive index (n) and extinction coefficient (k)) determined from the FTIR spectra in Figure 4, from the optical properties the dielectric function, the energy loss function Im (−1/ ε1(ω)) are determined for various calcination temperature for (a) ZnO/TiO2 (2.5 g) and (b) ZnO/TiO2 (5 g).

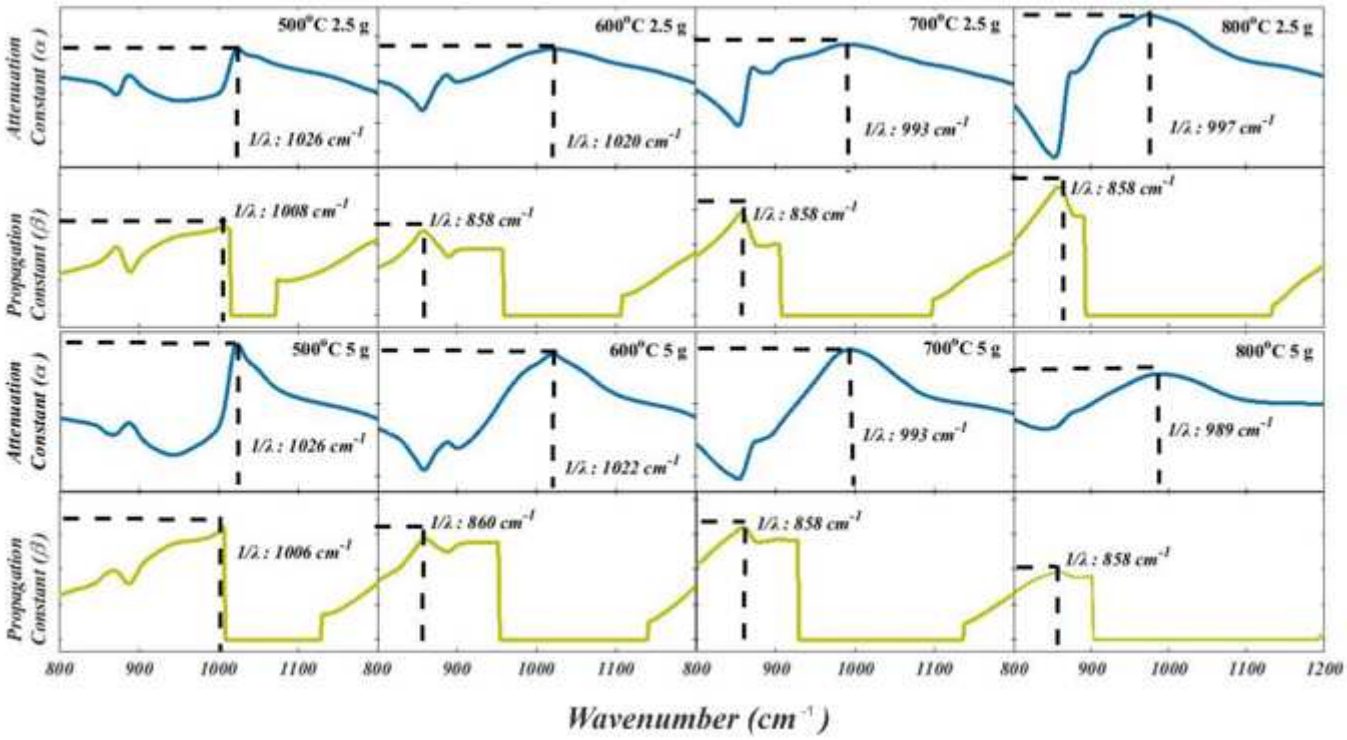

Figure 6

Attenuation constant (α) (first and third rows) and propagation constant (β) (second and fourth rows) as a function of the wavenumber for calcination temperature from 500oC (left) to 800oC (right). First and second rows for 2.5 gr of TiO2 in ZnO/TiO2 composite and the third and fourth rows for 5 gr of TiO2 in ZnO/TiO2 composite.

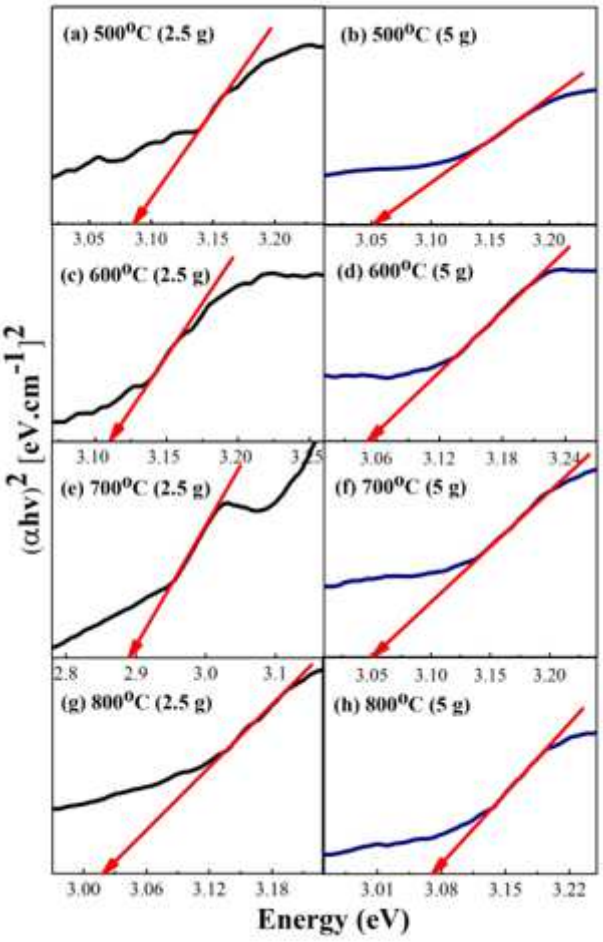

Figure 7

Band gap of ZnO/TiO2 synthesized from Calopogonium mucunoides leaves extract for various calcination temperature (500oC, 600oC, 700oC, 800oC) and TiO2 concentration (2.5 g and 5 g)

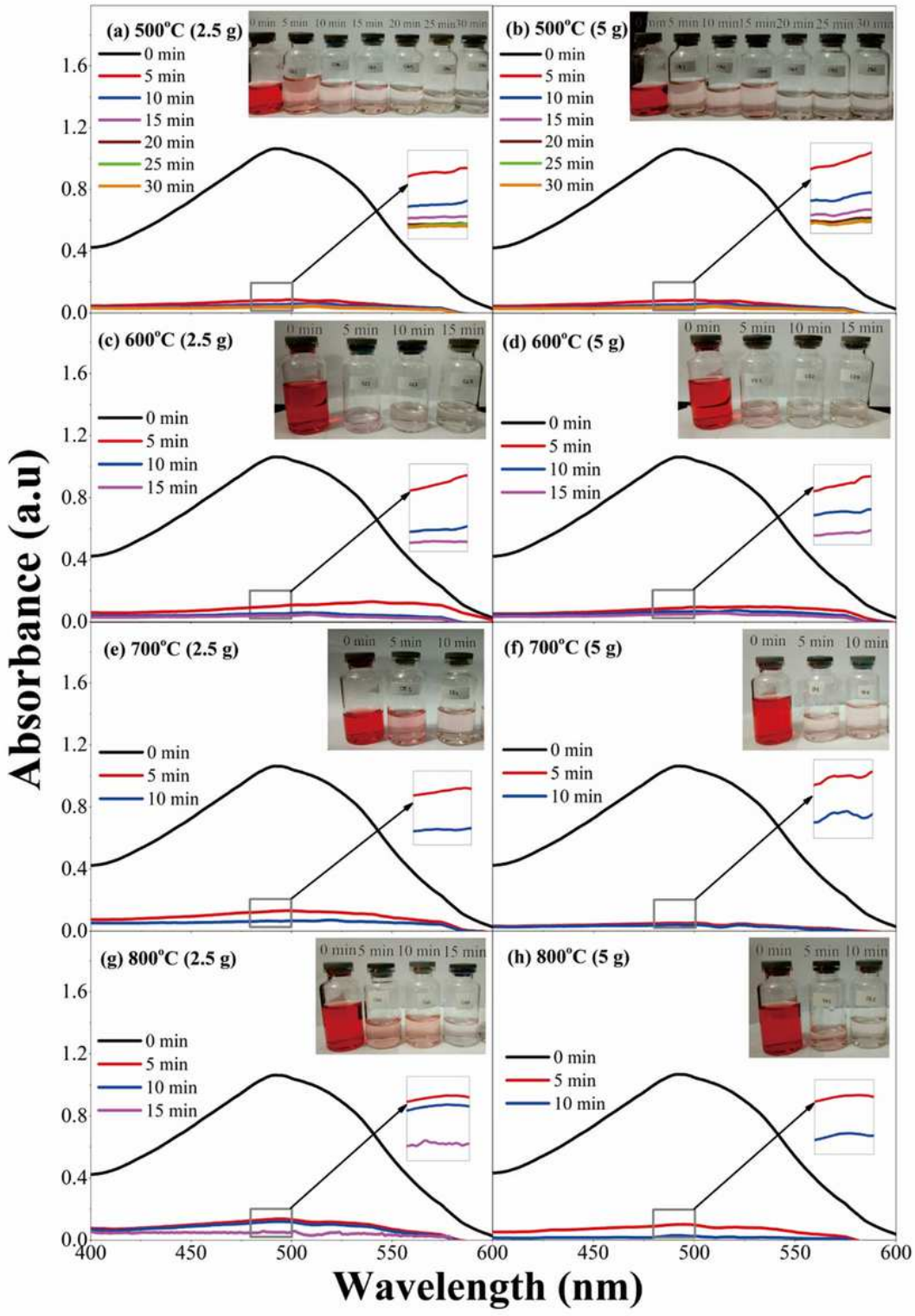

Figure 8

UV-visible absorption spectra of ZnO/TiO2 (2.5 g and 5 g) synthesized from Calopogonium mucunoides leaves extract for various calcination temperature (500oC, 600oC, 700oC, and 800oC)

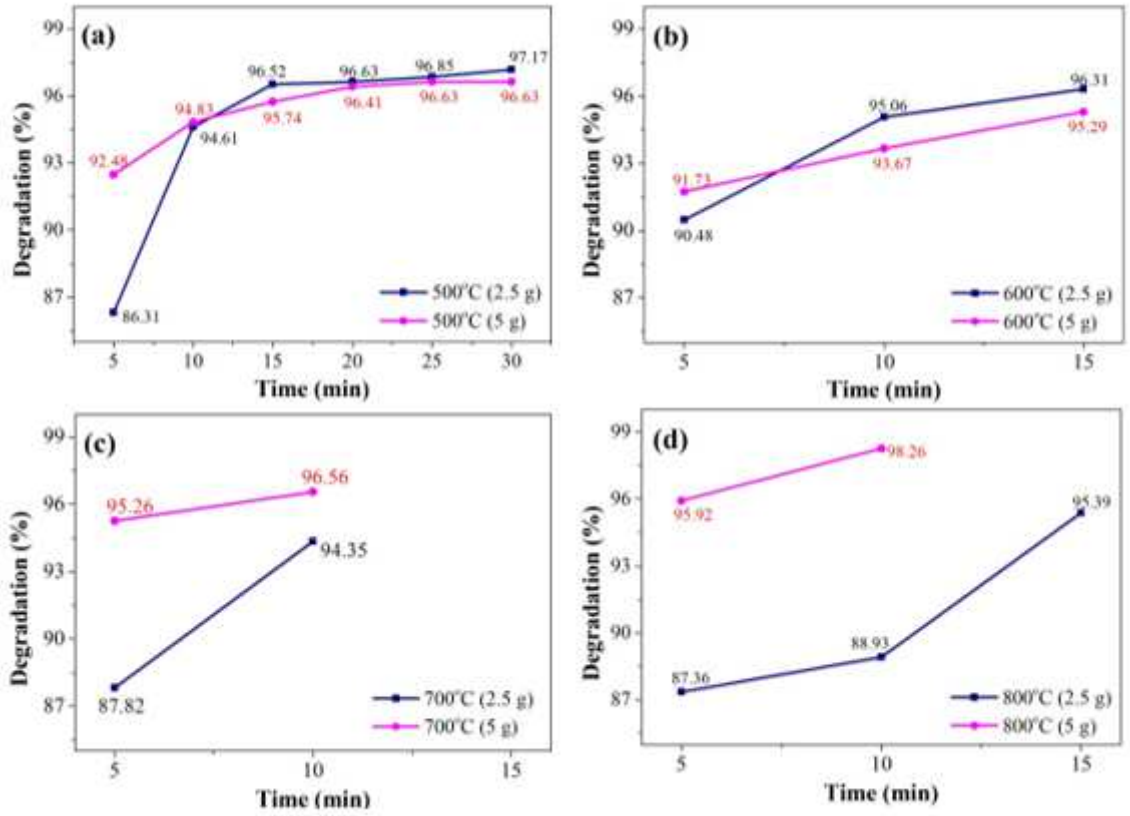

Figure 9

Percentage degradation of CR with the different catalysts (a) 500oC, (b) 600oC, (c) 700oC, and (d) 800oC

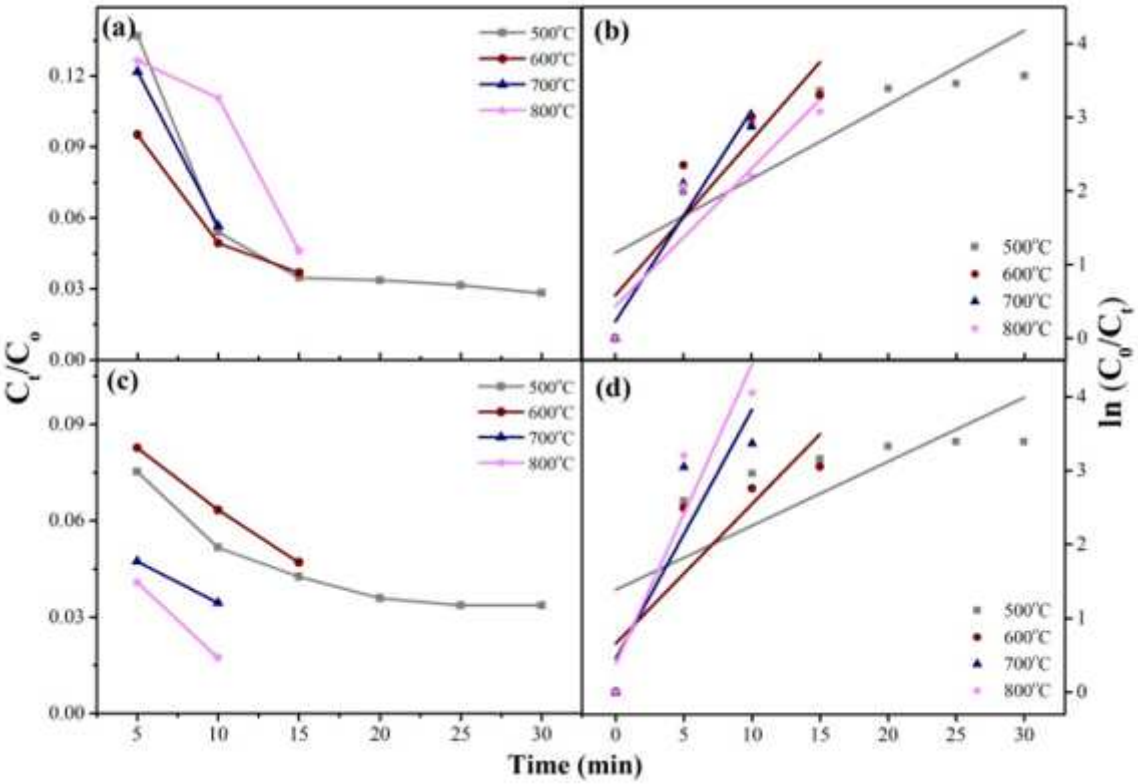

Figure 10

Photocatalytic performance and kinetic model of composites (a-b) ZnO/TiO2 (2,5 g) and (c-d) ZnO/TiO2 (5 g) for various calcination temperature in CR solution

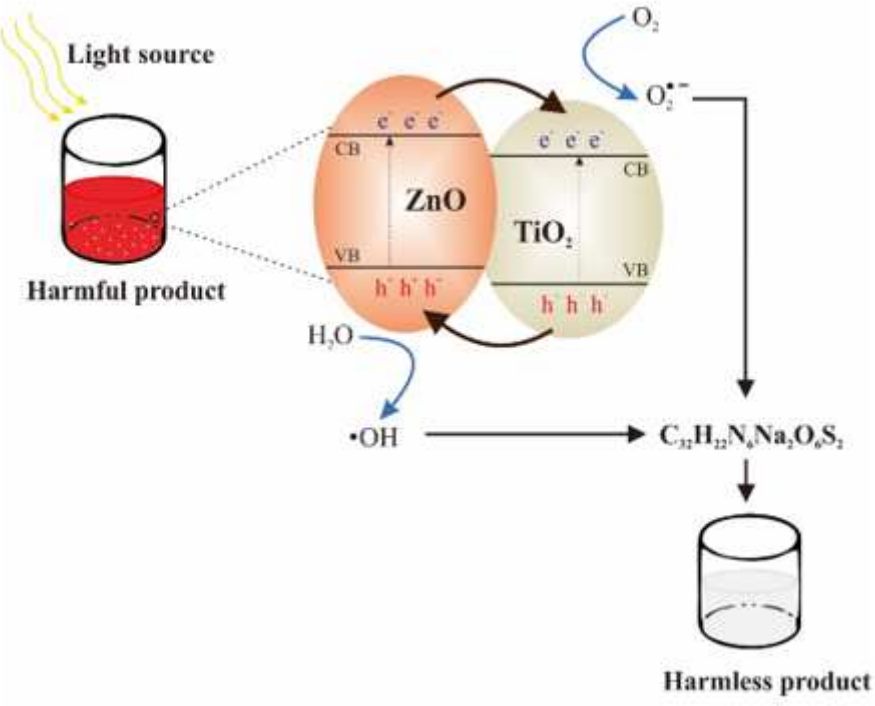

Figure 11

Schematic degradation process of CR from the incoming photon, transfer charge (electron and hole), produce radicals to break the bond of CR, and the final product of photocatalytic in the composite ZnO/TiO2

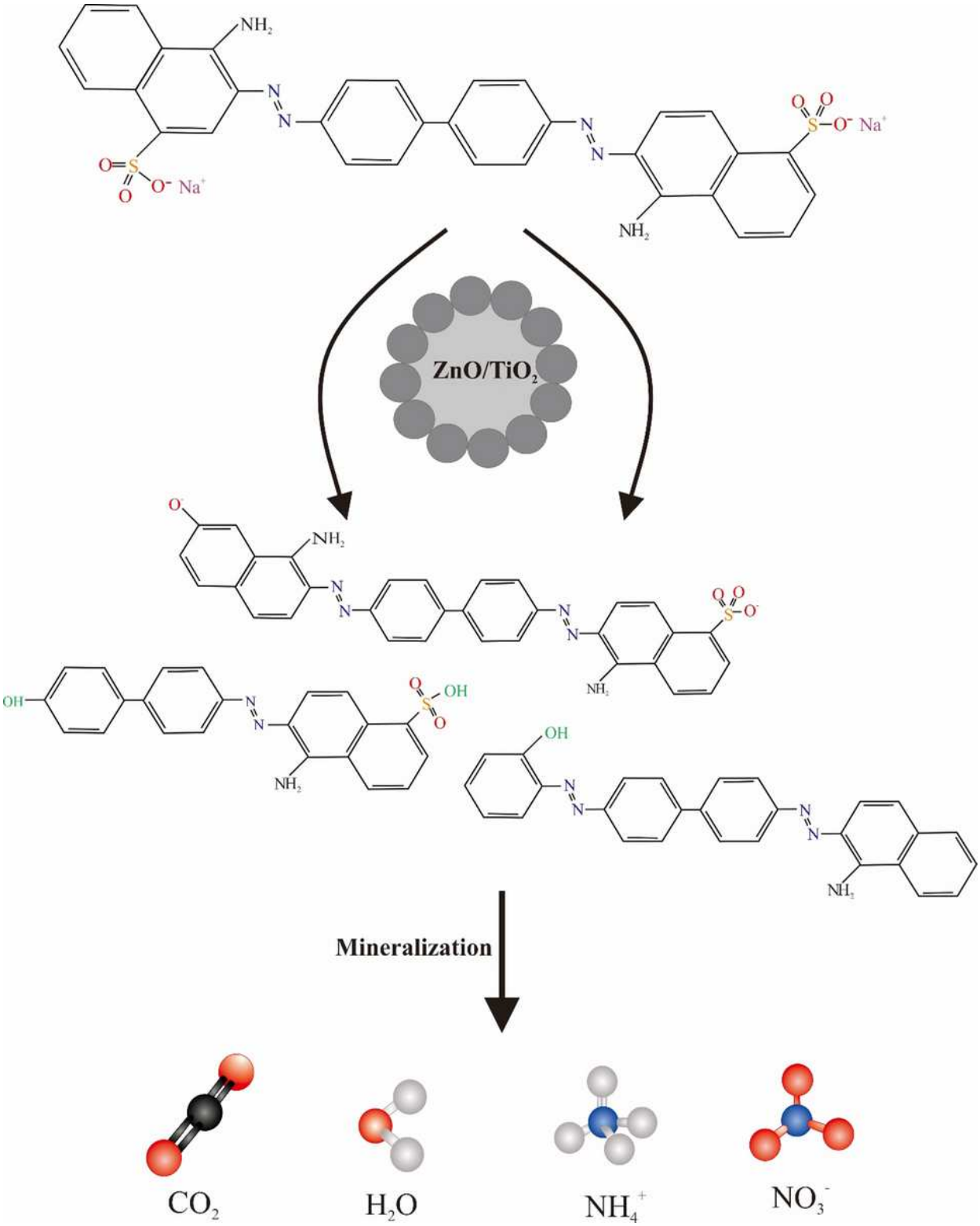

Figure 12

Demineralization mechanism of CR by the composite ZnO/TiO2 in the photodegradation process

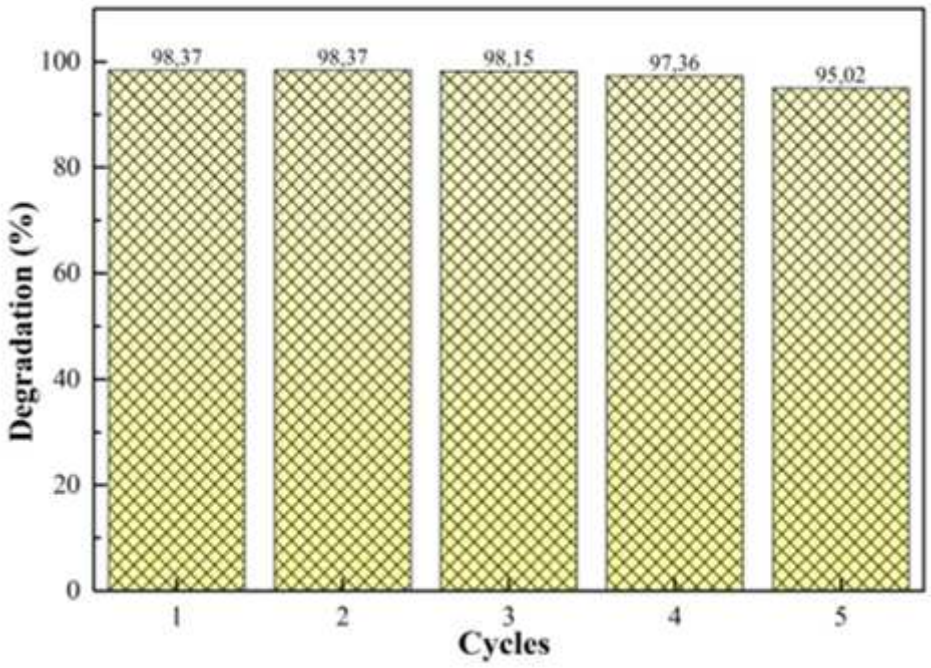

Figure 13

Stability degradation performance of composite ZnO/TiO2 for CR dye up to five times